MAXIMAL INTENSITY HIGHER-ORDER BREATHERS OF THE NONLINEAR SCHRÖDINGER EQUATION ON DIFFERENT BACKGROUNDS

An Undergraduate Research Scholars Thesis

by

OMAR A. ASHOUR

Submitted to the Undergraduate Research Scholars program
Texas A&M University
in partial fulfillment of the requirements for the designation as an

UNDERGRADUATE RESEARCH SCHOLAR

Approved by
Research Co-Advisor: Dr. Siu A. Chin
Research Co-Advisor: Dr. Milivoj R. Belić

May 2017

Major: Electrical Engineering

TABLE OF CONTENTS

ABSTRACT

Maximal Intensity Higher-Order Breathers of the Nonlinear Schrödinger Equation on Different Backgrounds

Omar A. Ashour
Department of Electrical and Computer Engineering
Texas A&M University

Research Co-Advisor: Dr. Siu A. Chin
Department of Physics and Astronomy
Texas A&M University

Research Co-Advisor: Dr. Milivoj R. Belić
Science Program
Texas A&M University at Qatar

In this work, we present fully periodic breathers of the nonlinear Schrodinger equation (NLSE) on both constant and elliptical dn-function backgrounds. The breathers can be generated under two conditions 1) the periods of the constituent breathers of the higher-order structures must be commensurate with each other; and 2) the period of the constituent first order breather must be commensurate with the period of the background. Breathers on constant backgrounds of arbitrary order can be generated numerically using a fully systematic procedure, pointing to the possibility of generating them experimentally using frequency combs. The peak height formula is presented and used to prove that these families of breathers are of maximal intensity.

DEDICATION

I would like to dedicate this manuscript to my parents and grandmother- Sawsan, Abdelwahed and Farida. Thank you for being here every step of the way the past 4 years while I worked on the projects that eventually lead to this thesis. Without your constant love and support, I would not be where I am or who I am today. You always egged me on when I almost gave up, and believed in me when I lost faith in myself. Your hard work and dedication to my future and wellbeing have been the cornerstone of everything I have accomplished so far. Grandma, thank you for always showing interest in my work and fostering a love of science and learning in me since childhood. Mom and dad, while you might jokingly roll your eyes at how much I've crossed over to the dark side of physics, thank you for everything you have taught me and for the half-decent genes.

I would also like to thank my siblings, Injy and Mazen, who are the most wonderful siblings I could ask for. I shall forgive you for the endless nerd bullying. Finally, I must thank my best friend, Laila Nasser, who has put up with my nerdy rants for the past 4 years. Thank you for proof reading my work and even faking interest in it, you will be a brilliant mathematician some day.

ACKNOWLEDGMENTS

First of all, I would like to start out by thanking my two wonderful advisors: Professors Siu Chin and Milivoj Belić. Professor Belić, thank you for giving me the chance to prove myself when I was merely a freshman who barely knew integral calculus. You allowed me to join your research group, and while I did not produce anything of value for the first year and a half, you still encouraged me and always answered my most basic questions. You introduced me to nonlinear optics and dynamics over 3 years ago, and to this day I am still captivated by this exciting field. Professor Chin, thank you for teaching me all I know about computational physics. You always tolerated my lack of knowledge, even in matters as basic as Fourier transforms when I first started. Your conscientiousness and thorough feedback have improved not only my scientific knowledge, but also my writing and figure preparation skills.

I would also like to thank other members of our research group, Branislav Aleksić and Dr. Stanko Nikolić. Branislav, thank you for being my first mentor, under your mentorship I have gone from barely understanding pointers in C to writing a full library for solving the NLSE on GPUs and clusters in a few months. Stanko, thank you for the many insightful and interesting discussions and for explaining some of theoretical concepts I was never exposed to before. I have very much enjoyed working with you and learned a great deal.

Last but not least, I would like to thank Professor Peter Rentzepis, my (physical chemist) mentor from electrical engineering. Professor Rentzepis, this thesis would not have been possible without your support and assistance. You put in so much effort into helping me achieve my goals, you never asked for anything in return besides “being good,” and I promise I’ll do my best. Thank you for the many lessons you taught me, on both life and science.

LIST OF ABBREVIATIONS

AB	Akhmediev Breather
ABn	*n*th-order Akhmediev breather
BCH	Baker-Campbell-Hausdorff
BEC	Bose-Einstein Condensate
DT	Darboux Transformation
FFT	Fast-Fourier Transform
MI	Modulation Instability
MPI	Multi-Product Integrators
NLSE	Nonlinear Schrödinger Equation
PHF	Peak-Height Formula
RW	Rogue Wave

CHAPTER I

INTRODUCTION

1. The Cubic Nonlinear Schrödinger Equation

The cubic (1+1)-dimensional nonlinear Schrödinger equation (NLSE) in dimensionless form is given as:

$$i\frac{\partial\psi}{\partial x}+\frac{1}{2}\frac{\partial^2\psi}{\partial t^2}+|\psi|^2\psi=0 \tag{1.1}$$

where x, t depend on the physical problem being studied. In optical fibers, x represents the distance along the fiber and t is the retarded time (i.e. in the frame moving at the group velocity of the pulse). ψ is the slowly varying pulse envelope [1]. The cubic NLSE (1.1) is a nonlinear evolution partial differential equation that naturally arises in multiple areas of physics and engineering including ocean surface wave [2, 3] and light propagation in nonlinear media, nonlinear lattices [1], optical fibers [4] and Bose-Einstein condensates [5].

The NLSE (1.1) can be written as the compatibility condition of the following linear system [6, 7]:

$$\begin{aligned}\boldsymbol{R}_t &= -\boldsymbol{JR\Lambda}+\boldsymbol{UR},\\ \boldsymbol{R}_x &= -\boldsymbol{JR\Lambda^2}+\boldsymbol{UR\Lambda}-\frac{1}{2}\left(\boldsymbol{JU^2}-\boldsymbol{JU_t}\right)\boldsymbol{R}\end{aligned} \tag{1.2}$$

where

$$\boldsymbol{R}=\begin{pmatrix} r_{11} & s^* \\ s & r_{22}\end{pmatrix},\ \boldsymbol{U}=\begin{pmatrix} 0 & \psi \\ \phi & 0\end{pmatrix}, \tag{1.3}$$

$$\boldsymbol{J}=\begin{pmatrix} i & 0 \\ 0 & -i\end{pmatrix},\ \boldsymbol{\Lambda}=\begin{pmatrix} \lambda & 0 \\ 0 & \lambda^*\end{pmatrix}. \tag{1.4}$$

This is known as the Zhakharov-Shabat system of (1.1), and λ is an eigenvalue. Note that the matrix Λ is isospectral, that is, $\frac{d\lambda}{dt}\equiv 0$. For the case of anomalous dispersion represented by (1.1), one can set $r_{22}=-r_{11}^*=-r^*$ and $\psi=-\phi^*$ [6].

Multiplying out (1.2), one obtains [6]:

$$\boldsymbol{R}_t = \begin{pmatrix} s\psi - ir\lambda & -\psi r^* - is^*\lambda^* \\ is\lambda - r\psi^* & -ir^*\lambda^* - s^*\psi^* \end{pmatrix},$$
$$\boldsymbol{R}_x = \begin{pmatrix} \lambda(s\psi - ir\lambda) + \frac{1}{2}ir\psi\psi^* + \frac{1}{2}is\psi_t & -\frac{1}{2}i\left(r^*\left(\psi_t - 2i\psi\lambda^*\right) + s^*\left(2\left(\lambda^*\right)^2 - \psi\psi^*\right)\right) \\ \frac{1}{2}i\left(2s\lambda^2 + (2ir\lambda - s\psi)\psi^* + r\left(\psi_t\right)^*\right) & -\frac{1}{2}i\left(r^*\left(2\left(\lambda^*\right)^2 - \psi\psi^*\right) + s^*\left(-2i\lambda^*\psi^* - \left(\psi_t\right)^*\right)\right) \end{pmatrix}. \tag{1.5}$$

It is straightforward to see that the first column of each matrix in (1.5) can be written as [6]:

$$\begin{aligned} R_t &= \boldsymbol{L}R, \\ R_x &= \boldsymbol{A}R, \end{aligned} \tag{1.6}$$

where

$$\boldsymbol{L} = \begin{pmatrix} -i\lambda & \psi \\ -\psi^* & i\lambda \end{pmatrix}, \ \boldsymbol{A} = \begin{pmatrix} -i\lambda^2 + i\frac{1}{2}|\psi|^2 & \lambda\psi + i\frac{1}{2}\psi_t \\ -\lambda\psi^* + i\frac{1}{2}\psi_t^* & i\lambda^2 - i\frac{1}{2}|\psi|^2 \end{pmatrix}, \ R = \begin{pmatrix} r \\ s \end{pmatrix} \tag{1.7}$$

The operators (matrices) $\boldsymbol{L}$ and $\boldsymbol{A}$ are known as the Lax pair of (1.1), and the functions $r(x,t)$ and $s(x,t)$ are the Lax pair generating functions. The compatibility condition of the differential equations equations (1.6) (also known as the zero-curvature condition from differential geometry) is $R_{tx} = R_{xt}$ [6, 8], leading to:

$$R_{tx} = \boldsymbol{L}_x R + \boldsymbol{L}R_x = R_{xt} = \boldsymbol{A}_t R + \boldsymbol{A}R_t, \tag{1.8}$$

thus,

$$\boldsymbol{L}_x R + \boldsymbol{L}\boldsymbol{A}R = \boldsymbol{A}_t R + \boldsymbol{A}\boldsymbol{L}R\,, \tag{1.9}$$

$$\boldsymbol{L}_x - \boldsymbol{A}_t - [\boldsymbol{A}, \boldsymbol{L}] = \boldsymbol{0}\,, \tag{1.10}$$

where $[\boldsymbol{A}, \boldsymbol{L}] \equiv \boldsymbol{AL} - \boldsymbol{LA}$ is the commutator. Computing the operators from (1.10), one gets:

$$\begin{aligned} \boldsymbol{L}_x - \boldsymbol{A_t} &= \begin{pmatrix} -\frac{1}{2}i\left(\psi^*\psi_t + \psi\psi_t^*\right) & \psi_x - \lambda\psi_t - \frac{1}{2}i\psi_{tt} \\ -\psi_x^* - \frac{1}{2}i\psi_{tt}^* + \lambda\psi_t^* & \frac{1}{2}i\left(\psi^*\psi_t + \psi\psi_t^*\right) \end{pmatrix} \\ [\boldsymbol{A}, \boldsymbol{L}] &= \begin{pmatrix} -\frac{1}{2}i\left(\psi^*\psi_t + \psi\psi_t^*\right) & i\left|\psi\right|^2\psi - \lambda\psi_t \\ i\left|\psi\right|^2\psi^* + \lambda\psi_t^* & \frac{1}{2}i\left(\psi^*\psi_t + \psi\psi_t^*\right) \end{pmatrix} \end{aligned} \tag{1.11}$$

Consequently, substituting in (1.10), one gets:

$$\boldsymbol{L}_x - \boldsymbol{A}_t - [\boldsymbol{A}, \boldsymbol{L}] = \begin{pmatrix} 0 & i\psi_x + \frac{1}{2}\psi_{tt} + \left|\psi\right|^2\psi \\ -i\psi_x^* + \frac{1}{2}\psi_{tt}^* + \left|\psi\right|^2\psi^* & 0 \end{pmatrix} = \boldsymbol{0}\,, \tag{1.12}$$

that is, (1.1) and its complex conjugate.

1.1. Breather Solutions

Breathers are a large family of periodic solutions of the nonlinear Schrodinger equation which have been extensively studied theoretically [9–12], numerically [9, 13] and even experimentally [14, 15]. Higher order breathers can be easily studied using the Darboux transformation, as will be discussed in the next section. Two main types of breathers exist: Akhmediev breathers (ABs) and Kuznetsov-Ma breathers (KMBs). Examples of breathers are shown in Fig. 1.1. Since this thesis deals mainly with Akhmediev breathers, their discussion will be postponed to Chapter III for constant backgrounds and Chapter V for elliptic function backgrounds.

1.1.1. Rogue Waves

Research into rogue waves is an emerging topic of interest [16–18]. They appear in studies of ocean waves [19, 20], Bose-Einstein condensates [21], optics [4, 22, 23] and even superfluids [24]. Optical rogue waves can be regarded as a special case of Akhmediev breathers when $L \to \infty$, where L represents the period of the breather [25]. In this context, the first order rogue wave is the Peregrine soliton [26] shown in Fig. 1.2 (a). A rational second order rogue wave [25, 27] is shown in Fig. 1.2 (b).

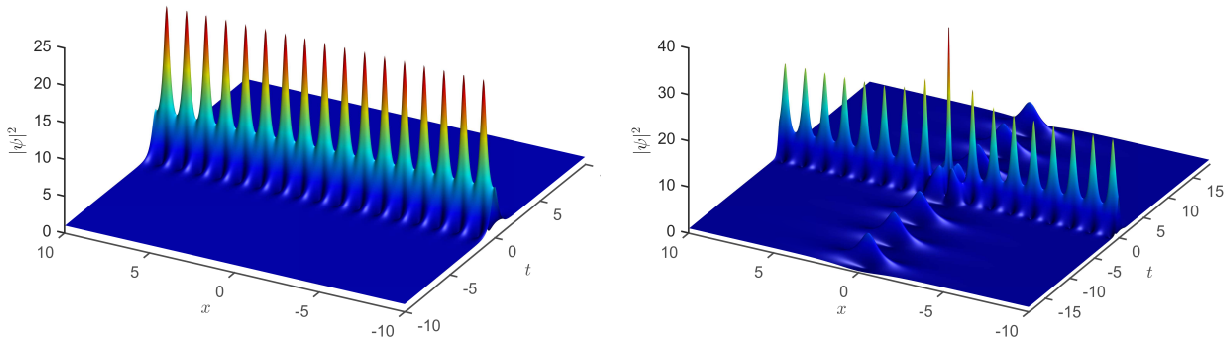

(a) (b)

Fig. 1.1: (a) A first-order KMB at $\lambda = 1.8i$. (b) collison of first-order AB with $\lambda = 0.8i$ and a KMB with $\lambda = 1.8i$, leading to a second-order breather at the point of collision.

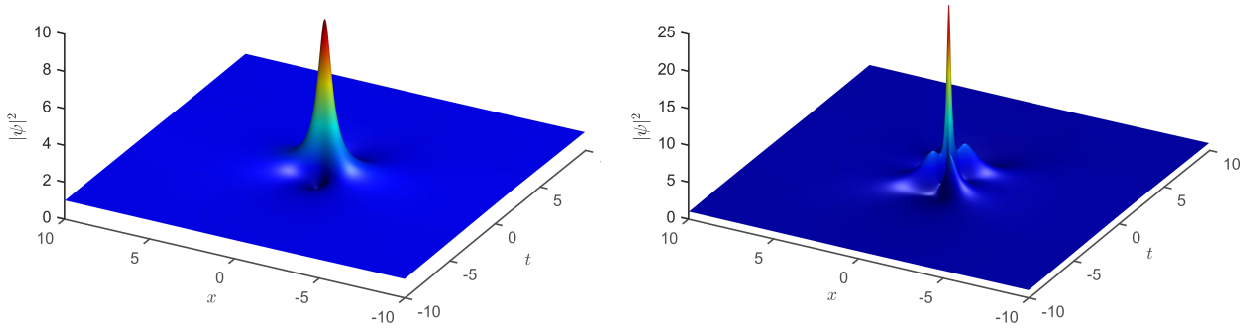

(a) (b)

Fig. 1.2: (a) A Peregrine soliton (1st order RW). Peak intensity is 9. (b) A rational second order RW. Peak intensity is 25.

1.2. Soliton Solutions

Solitons are self-focusing wave-packets which maintain their shape during propagation. They arise in nonlinear PDEs due to a balance between dispersive and nonlinear effects. Soliton solutions of nonlinear Schrödinger equations are some of the most extensively studied solitons in the literature

[28–32]. Soliton solutions of (1.1) on a cnoidal background have also been studied by Kedziora *et al.* [12]. An example of a first-order soliton is shown in Fig. 1.3.

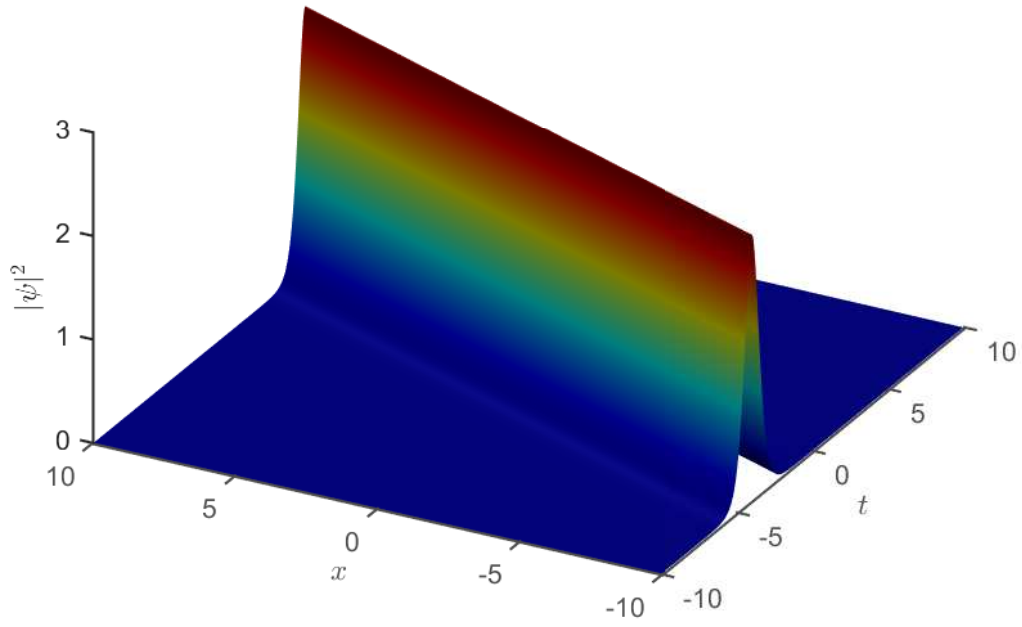

Fig. 1.3: A first-order soliton at $\lambda = 0.2 + 0.8i$. Peak intensity is 2.56.

2. The Darboux Transformation

Given some solution of the Zhakharov-Shabat (ZS) system (1.2) $\boldsymbol{R_1}$ corresponding to some eigenvalue λ_1, and a different solution $\boldsymbol{R_0}$ corresponding to a different eigenvalue λ_0, it is well known that the ZS system (1.2) is covariant under the following transformation [6, 7]:

$$\begin{aligned} \boldsymbol{R}_2 &= \boldsymbol{R}_1\boldsymbol{\Lambda} - \boldsymbol{\sigma}\boldsymbol{R}_1\,, \\ \boldsymbol{U}_2 &= \boldsymbol{U}_1 + [\boldsymbol{J}, \boldsymbol{\sigma}]\,, \end{aligned} \tag{1.13}$$

where $\sigma = \boldsymbol{R}_0\boldsymbol{\Lambda}\boldsymbol{R}_0^{-1}$.

The term covariant means that $\boldsymbol{R_2}$ is also solution of (1.2) (or its first column a solution of the equivalent Lax system (1.6)). Consequently, starting out with two known solutions ψ_0, ψ_1 of the NLSE (1.1), the Zhakharov-Shabat system (1.2) can be solved to obtain the corresponding solutions $\boldsymbol{R_0}, \boldsymbol{R_1}$. One can then obtain a different solution using the Darboux Transformation (DT) (1.13), which can then be extracted from U_2. Conventionally, the DT is used with some well-known background (or "seed") solutions of the NLSE, shown in table 1.1. Note that these solutions are all independent of the eigenvalue λ, and thus $\boldsymbol{R_1}$ can be used as $\boldsymbol{R_0}$.

Starting from an initial background (or seed) solution ψ_0, one can find $\boldsymbol{\sigma}$:

$$\boldsymbol{\sigma} = \begin{pmatrix} \Delta(|r|^2\lambda + |s|^2\lambda^*) & \Delta(rs^*(\lambda - \lambda^*)) \\ \Delta(sr^*(\lambda - \lambda^*)) & \Delta(|s|^2\lambda + |r|^2\lambda^*) \end{pmatrix}, \tag{1.14}$$

where $\Delta = (|r|^2 + |s|^2)^{-1}$

Consequently, $\boldsymbol{U}_2$ takes the form:

$$\boldsymbol{U_2} = \begin{pmatrix} 0 & \psi_0 + \Delta(2irs^*(\lambda - \lambda^*)) \\ -\psi_0 - \Delta(2isr^*(\lambda - \lambda^*)) & 0 \end{pmatrix} \tag{1.15}$$

Generalizing the last result, one obtains the well known DT equation [6, 7, 27, 33]:

$$\psi_n = \psi_0 + \sum_{m=1}^{n} \frac{2ir_{m1}s^*_{m1}(\lambda_m - \lambda^*_m)}{|r_{m1}|^2 + |s_{m1}|^2} \tag{1.16}$$

The recursive relations for obtaining the higher-order Lax pair generating functions r and s follow from (1.13):

Table 1.1: Seed solutions of the cubic NLSE (1.1)

Seed solution (ψ_0)	Higher-order solutions
$\psi_0 = 0$	Solitons [6, 34]
$\psi_0 = e^{ix}$	Breathers [6, 35]
$\psi_0 = \mathrm{dn}(t - t_0, k)e^{i(x-x_0)(1-\frac{k^2}{2})}$,	Breathers and rogue waves on dn background [12]
$\psi_0 = k\mathrm{cn}(t - t_0, k)e^{i(x-x_0)(k^2-\frac{1}{2})}$	Solitons and rogue waves on cn background [12]

$$
\begin{aligned}
r_{nj} = &[(l^*_{n-1} - l_{n-1}) s^*_{n-1,1} r_{n-1,1} s_{n-1,j+1} \\
&+ (l_{j+n-1} - l_{n-1}) |r_{n-1,1}|^2 r_{n-1,j+1} \\
&+ (l_{j+n-1} - l^*_{n-1}) |s_{n-1,1}|^2 r_{n-1,j+1}] / (|r_{n-1,1}|^2 + |s_{n-1,1}|^2), \qquad (1.17) \\
s_{nj} = &[(l^*_{n-1} - l_{n-1}) s_{n-1,1} r^*_{n-1,1} r_{n-1,j+1} \\
&+ (l_{j+n-1} - l_{n-1}) |s_{n-1,1}|^2 s_{n-1,j+1} \\
&+ (l_{j+n-1} - l^*_{n-1}) |r_{n-1,1}|^2 s_{n-1,j+1}] / (|r_{n-1,1}|^2 + |s_{n-1,1}|^2). \qquad (1.18)
\end{aligned}
$$

3. Solving NLSE Numerically

3.1. Symplectic Integrators

Equation (1.1) can be written as:

$$
-i \frac{\partial \psi}{\partial x} = \left(\hat{D} + \hat{N} \right) \psi \qquad (1.19)
$$

where the operator $\hat{D} = \frac{1}{2} \frac{\partial^2}{\partial t^2}$ represents the dispersion operator in the medium and $\hat{N} = |\psi|^2$ the nonlinearity. Evolving $\psi(x,t)$ one step forward in x to $\psi(x + \Delta x, t)$ can be formally written as:

$$
\psi(x + \Delta x, t) = \mathrm{e}^{\epsilon(\hat{D} + \hat{N})} \psi(x,t) \qquad (1.20)
$$

where $\epsilon = i \Delta x$. For some positive integer n, and since the operators $\hat{D}$ and $\hat{N}$ do not commute,

$$
\mathrm{e}^{(\hat{D} + \hat{N})\epsilon} = \prod_{i=1}^{k} \mathrm{e}^{c_i \hat{D} \epsilon} \mathrm{e}^{d_i \hat{N} \epsilon} + \mathcal{O}(\epsilon^{n+1}) \qquad (1.21)
$$

for some constants c_i and d_i. Since the separate nonlinear and dispersion equations are exactly solvable, this is an efficient way of approximating the solution. Note that the action of the dispersion operator is easily computed in Fourier space, so fast-Fourier transforms are used when these integrators are implemented numerically. Recalling the Baker-Campbell-Hausdorff (BCH) formula [36–38].

$$
\exp(Z) = \exp(X) \exp(Y) \qquad (1.22)
$$

where

$$
\begin{aligned}
Z = X + Y + \frac{1}{2}[X,Y] \\
&+ \frac{1}{12}\left([X,[X,Y]] + [Y,[Y,X]]\right) - \frac{1}{24}[Y,[X,[X,Y]]] \\
&- \frac{1}{720}\left([Y,[Y,[Y,[Y,X]]]] + [X,[X,[X,[X,Y]]]]\right) \\
&+ \frac{1}{360}\left([X,[Y,[Y,[Y,X]]]] + [Y,[X,[X,[X,Y]]]]\right) \\
&+ \frac{1}{120}\left([Y,[X,[Y,[X,Y]]]] + [X,[Y,[X,[Y,X]]]]\right) + \cdots
\end{aligned}
\tag{1.23}
$$

Applying (1.22) and (1.23) to (1.21) with $k = 1.$, one obtains:

$$
\begin{aligned}
(\hat{D} + \hat{N})\epsilon &= c_1\hat{D} + d_1\hat{N} + \epsilon^2\frac{c_1 d_1}{2}[\hat{D},\hat{N}] + \cdots \\
&= c_1\hat{D} + d_1\hat{N} + \mathcal{O}(\epsilon^2)
\end{aligned}
\tag{1.24}
$$

it follows that $n = 1$ and $c_1 = d_1 = 1$. To obtain a higher order integrator, one needs to repeatedly apply (1.22) as follows:

$$
\exp(W) = \exp(c_1 X)\exp(d_1 Y)\exp(c_2 X) \tag{1.25}
$$

where

$$
W = (c_1 + c_2)X + d_1 Y - \frac{c_1 c_2 d_1}{6}[X,[X,Y]] + \frac{d_1^2 c_1}{6}[Y,[Y,X]] + \cdots \tag{1.26}
$$

Applying this to (1.21), one obtains:

$$
\begin{aligned}
(\hat{D} + \hat{N})\epsilon &= (c_1 + c_2)\hat{D} + d_1\hat{N} - \epsilon^3\left(\frac{c_1 c_2 d_1}{6}[X,[X,Y]] - \frac{d_1^2 c_1}{6}[Y,[Y,X]]\right) + \cdots \\
&= (c_1 + c_2)\hat{D} + d_1\hat{N} + \mathcal{O}(\epsilon^3)
\end{aligned}
\tag{1.27}
$$

and consequently, $c_1 = c_2 = \frac{1}{2}$ and $d_1 = 1, d_2 = 0$, with $n = 2$, leading to a second order symplectic integrator.

The coefficients of a fourth order integrator were derived by Forest and Ruth, one possibility is [37, 38]:

$$\begin{aligned} c_1 = c_2 = \frac{1}{2\left(2-2^{1/3}\right)}\,,\; c_3 = c_4 = \frac{1-2^{1/3}}{2\left(2-2^{1/3}\right)} \\ d_1 = d_3 = \frac{1}{2-2^{1/3}}\,,\; d_2 = \frac{2}{\left(2-2^{1/3}\right)}\,,\; d_4 = 0 \end{aligned} \tag{1.28}$$

Methods for deriving the coefficients of higher order integrators are given in [37].

3.2. Multi-product Integrators

Multi-product integrators (MPIs) were first demonstrated by Chin [39], and are especially powerful due to the smaller number of force evaluations (and consequently, fast-Fourier transforms) required, making them much quicker than symplectic integrators at higher orders. At sufficiently higher-orders MPIs are as accurate as symplectic integrators to machine precision.

CHAPTER II

PEAK HEIGHT FORMULA

The results derived in this chapter are originally given by us in Ref. [40] for the general case and Ref. [41] for ABs on a constant background. In this chapter, it will be shown that the peak height of any n^{th} order solution of the NLSE can be written as:

$$\psi_n(0,0) = \psi_0(0,0) + 2\sum_{m=1}^{n} \nu_m \tag{2.1}$$

if

$$s_{n1}(0,0) = e^{i\phi} r_{n1}(0,0) \tag{2.2}$$

where $\psi_0(0,0)$ is the seed wavefunction at the origin, r, s are the lax pair generating functions and ϕ is a phase.

First we prove that if the initial Lax pair generating functions obey the condition:

$$s_{1j}(0,0) = e^{i\phi} r_{1j}(0,0), \tag{2.3}$$

then (2.2) is also automatically satisfied. Since the functions r and s depend on the specific seed solution used in the Darboux transformation, we will just assume that (2.3) is true during this chapter, then it will be proved for the individual seeds in Chapters III and V.

We apply the recursive relations (1.17) and (1.18) at $x = t = 0$ and suppress the notation $(0,0)$. Starting from (2.3), one can prove that $s_{2j} = e^{i\phi} r_{2j}$ for $1 \leq j \leq N-1$, $s_{3j} = e^{i\phi} r_{3j}$ for $1 \leq j \leq N-2$, *etc.*. Therefore, given $s_{n-1,j} = e^{i\phi} r_{n-1,j}$, the recursion equations read:

$$\begin{aligned} r_{nj} &= -(ie^{-i\phi})\nu_{n-1}\, s_{n-1,j+1} + i\nu_{j+n-1}\, r_{n-1,j+1}, \\ s_{nj} &= (-ie^{i\phi})\nu_{n-1}\, r_{n-1,j+1} + i\nu_{j+n-1}\, s_{n-1,j+1}, \end{aligned} \tag{2.4}$$

which leads to:

$$\begin{aligned} e^{i\phi} r_{nj} &= -i\nu_{n-1} s_{n-1,j+1} + i\nu_{j+n-1}(e^{i\phi} r_{n-1,j+1}) \\ &= (-ie^{i\phi})\nu_{n-1}\, r_{n-1,j+1} + i\nu_{j+n-1}\, s_{n-1,j+1} \\ &= s_{nj}. \end{aligned} \tag{2.5}$$

Thus, we have proved by induction that (2.2) is true if (2.3) is also true.

In our work [40], we prove that (2.3) is true for all solutions of the NLSE of the form:

$$\psi_0(x,t) = AF(t)e^{iBx}, \tag{2.6}$$

given that $F(0) = 1$ and $F_t(0) = 0$. This includes all seed solutions shown in Table 1.1.

The peak height of NLSE solutions $|\psi(0,0)|$ has been studied previously. For example, Akhmediev and Mitzkevich [34] state a formula similar to our PHF (2.1) for solitons, but without giving a proof. In 2014, Kedziora *et al.* [12] have found that the peak height of "fused" RWs of order n with identical eigenvalues is as our formula predicts. Moreover, this was found to be true in Breather-to-soliton conversion in the quintic equation of the nonlinear-Schrödinger (NLS) hierarchy [42]. However, it should be mentioned that in none of these cases was the PHF derived or proved, it was simply observed to work for some special cases empirically or numerically.

CHAPTER III

MAXIMAL INTENSITY BREATHERS ON A CONSTANT BACKGROUND

In this chapter, we will introduce the first maximal intensity family studied in this thesis: breathers on a constant background. Breathers on a constant background correspond to a plane wave seed (constant background) solution of (1.1), $\psi_0 = e^{ix}$. In this case, the lax pair generating functions take the form [27]:

$$\begin{aligned} r_{1m} &= 2ie^{-ix/2}\sin(A), \\ s_{1m} &= 2e^{ix/2}\cos(B), \end{aligned} \tag{3.1}$$

where A and B are complex and given by:

$$A = \chi_m + \frac{1}{2}(\kappa_m(t-t_j) + d_j(x-x_m)) - \frac{\pi}{4}, \tag{3.2}$$

$$B = -\chi_m + \frac{1}{2}(\kappa_m(t-t_j) + d_j(x-x_m)) - \frac{\pi}{4}. \tag{3.3}$$

Here, $\kappa_m = 2\sqrt{1+\lambda_m^2}$ is the wavenumber of the m^{th} component, t_m and x_m are its x and t shifts respectively, and $d_m = \lambda_m\kappa_m$ and is closely related to the growth rate of the Fourier modes, as will be shown later in this chapter. In this case, $\chi_m = 1/2\arccos(\kappa_m/2)$. Generally, $\lambda_m = v_m + i\nu_m$ is the complex valued eigenvalue, where the real part v_m is the velocity of the m^{th} breather. An example of a first order breather with a complex eigenvalue is shown in Fig. 3.1

1. Breathers with a Purely Imaginary Eigenvalue

In this work, we restrict ourselves to breathers with a purely imaginary eigenvalue $\lambda_m = i\nu_m = i\sqrt{2a_m}$. The introduction of the parameter $0 < a_m < 0.5$ simplifies the arithmetic. Note that χ_m and κ_m are also real in this range of a_m. The Lax pair generating functions take the same form as (3.1), and $\kappa_m = 2\sqrt{1-2a}$. The t-period of the breathers is:

$$L = \frac{2\pi}{\kappa} = \frac{\pi}{\sqrt{1-2a}} \tag{3.4}$$

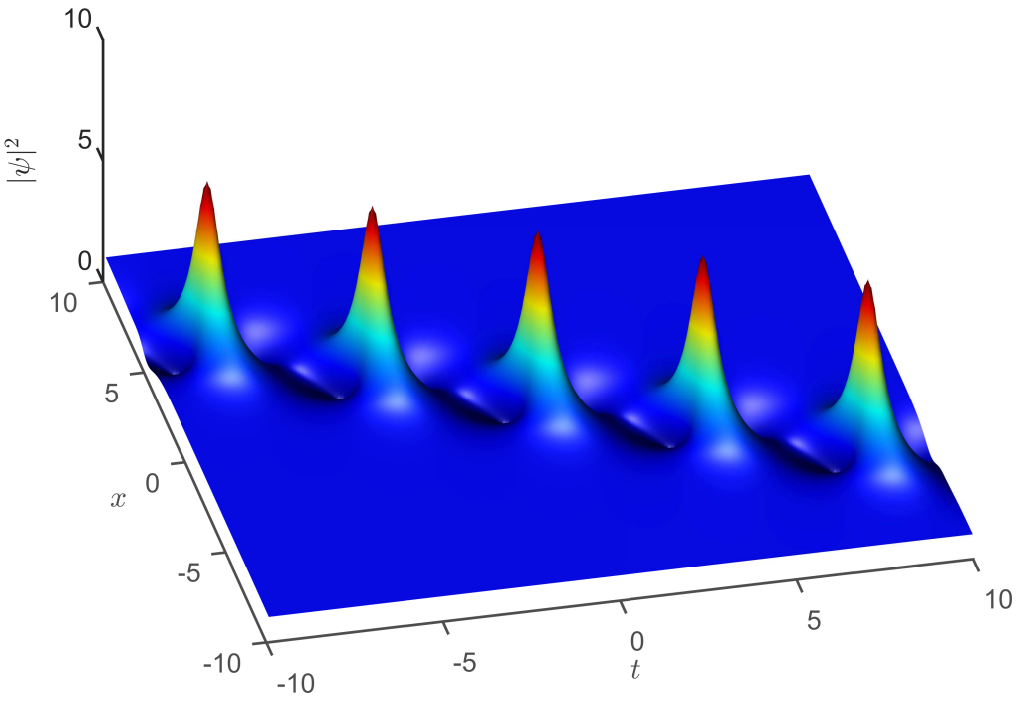

Fig. 3.1: A first order AB with a complex eigenvalue $\lambda_1 = 0.3 + 0.9i$. The veclocity controls the tilt angle between the line of breathers and the t-axis.

A and B at the origin ($x = t = 0$) for unshifted breathers ($x_m = t_m = 0$) have the form:

$$A(0,0) = \chi_m - \pi/4, \quad , B(0,0) = -\chi_m - \pi/4. \tag{3.5}$$

Consequently, r_{1m} and s_{1m} at the origin simplify to:

$$r_{1m}(0,0) = 2i\sin(\chi_m - \pi/4) = i\sqrt{2}\,(\sin\chi_m - \cos\chi_m) \tag{3.6}$$

$$s_{1m}(0,0) = 2\cos(\chi_m + \pi/4) = -\sqrt{2}\,(\sin\chi_m - \cos\chi_m) \tag{3.7}$$

which leads to $s_{1m}(0,0) = ir_{im}(0,0)$. From (2.3), we have proved that this family of solutions obeys the PHF (2.1). In this case, the peak-height formula takes the form:

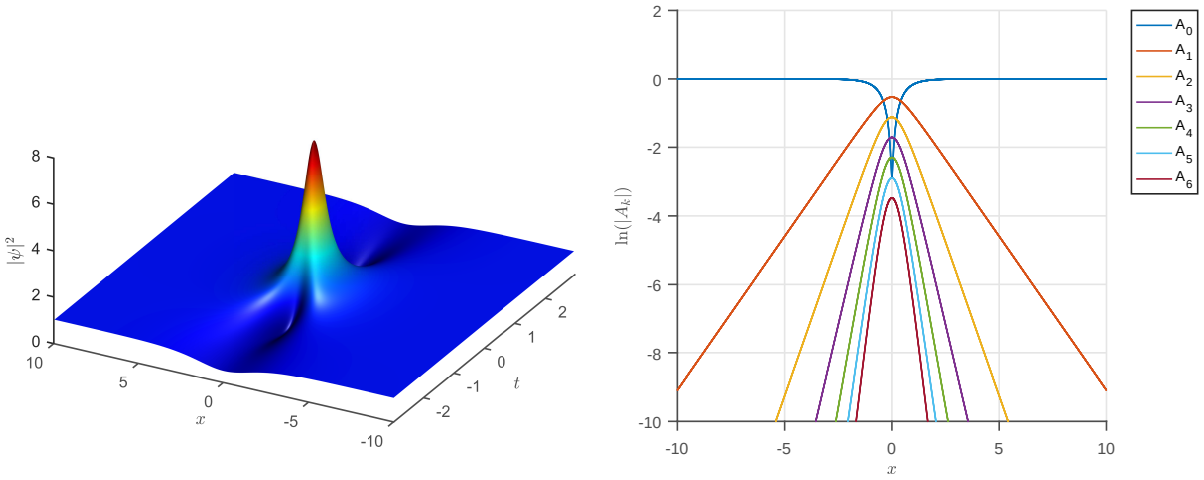

(a) (b)

Fig. 3.2: First order breather at $a = 0.36$ (a) and its spectrum (b). The mode A_1 in the spectrum has a growth rate of δ, while the mode A_2 grows like 2δ. In general, for first order breathers with one unstable mode, A_k grows like $k\delta$, locked to the first mode [9]. The peak height formula predicts an intensity of $(1 + 2\sqrt{2 \times 0.36})^2 \approx 7.27$, same as that produced by the numerical DT.

$$\psi_n(0,0) = 1 + 2\sum_{m=1}^{n} \sqrt{2a_m} \tag{3.8}$$

The first order breather, known as the Akhmediev breather, takes the form [11]:

$$\psi_1(x,t) = \left[\frac{(1-4a)\cosh(\delta x) + \sqrt{2a}\cos(\kappa t) + i\delta\sinh(\delta x)}{\sqrt{2a}\cos(\kappa t) - \cosh(\delta x)}\right] \mathrm{e}^{ix}, \tag{3.9}$$

where $\delta = \sqrt{2a}\kappa = \sqrt{8a(1-2a)}$ is the imaginary part of the parameter d_m occurring in (3.1) and gives the growth rate of the first mode in the Fourier spectrum of the Akhmediev breather. Such a breather and its spectrum are shown in Fig. 3.2.

2. Deriving The Maximal Intensity Family

When one attempts to generate a higher order breather using the Darboux transformation, one generally selects some values of a_m (or more generally, λ_m) and computes the resultant solution. However, in general, breathers of order 2 or higher completely lose their periodicity in this process. They are char-

acterized by a central ABn peak in the middle of the tx-plane, followed by "ripples" at higher values of t, as shown in Fig. 3.7. The characteristic periodicity of breathers is no longer present. Consequently, we seek to construct higher order breathers which are fully periodic, following the method we presented in our published work in Ref. [41]. To achieve this periodicity, the periods of the constituent breathers must be commensurate with each other. We select:

$$mL_m = L \Rightarrow \kappa_m = m\kappa \tag{3.10}$$

where $\kappa \equiv \kappa_1$. Simplifying this:

$$\sqrt{1-2a_m} = m\sqrt{1-2a} \tag{3.11}$$

$$a_m = m^2\left(a - \frac{1}{2}\right) + \frac{1}{2} \tag{3.12}$$

where $a \equiv a_1$. This very simple formula gives the relation between the a_m's required to generate these fully periodic higher order breathers

Fig. (3.3) shows a plot of the different a_m as a function of a. It is clear that there's a cut off, a_m^*, for each a_m, before which $a_m < 0$ and this invalid. This can be found by setting Eq. (3.12) to 0 and solving for a_m^*. The solution is:

$$a_m^* = \frac{1}{2}\left(1 - \frac{1}{m^2}\right) \tag{3.13}$$

A plot of the peak-heights of these breathers (as given by Eq. (3.8)) is shown in Fig. 3.4. It can be seen that they have continuous peak heights, so one can find a fully periodic breather of any intensity one requires. Fig. 3.5 and Fig. 3.6 show several fully periodic breathers whose a_m's are given by (3.12). It is very clear that these ABs are fully periodic, with no other peaks present besides the ABn peaks of interest. Note that the side peaks *appear* slightly shorter than the middle peak because they are extremely thin, requiring a very fine grid to plot them accurately. Contrast this to Fig. 3.7, which shows three "periods" of ABs, with the values of a_m slightly tuned from those obtained from Eq. (3.12). The result is clearly aperiodic, with multiple "ripples" that resemble AB1 peaks present.

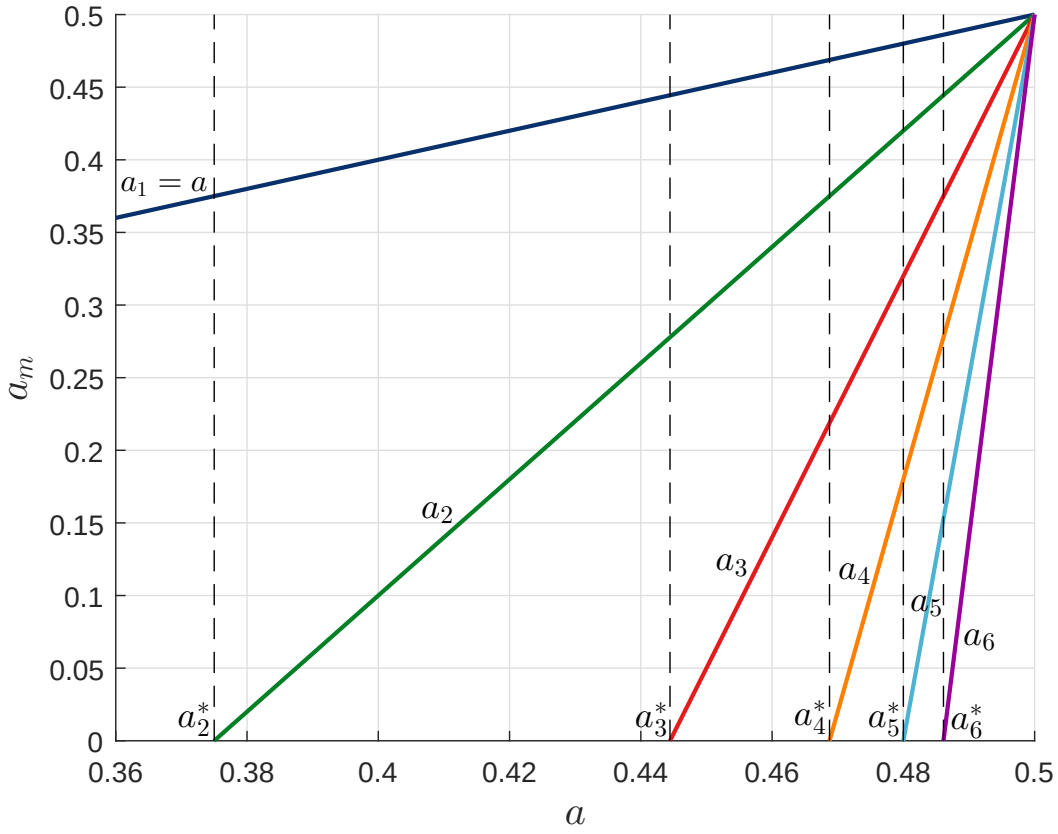

Fig. 3.3: Plot of the modulation parameters a_m as a function of a, as given by Eq. (3.12). Horizontal lines are the a_m^* given by Eq. (3.13)

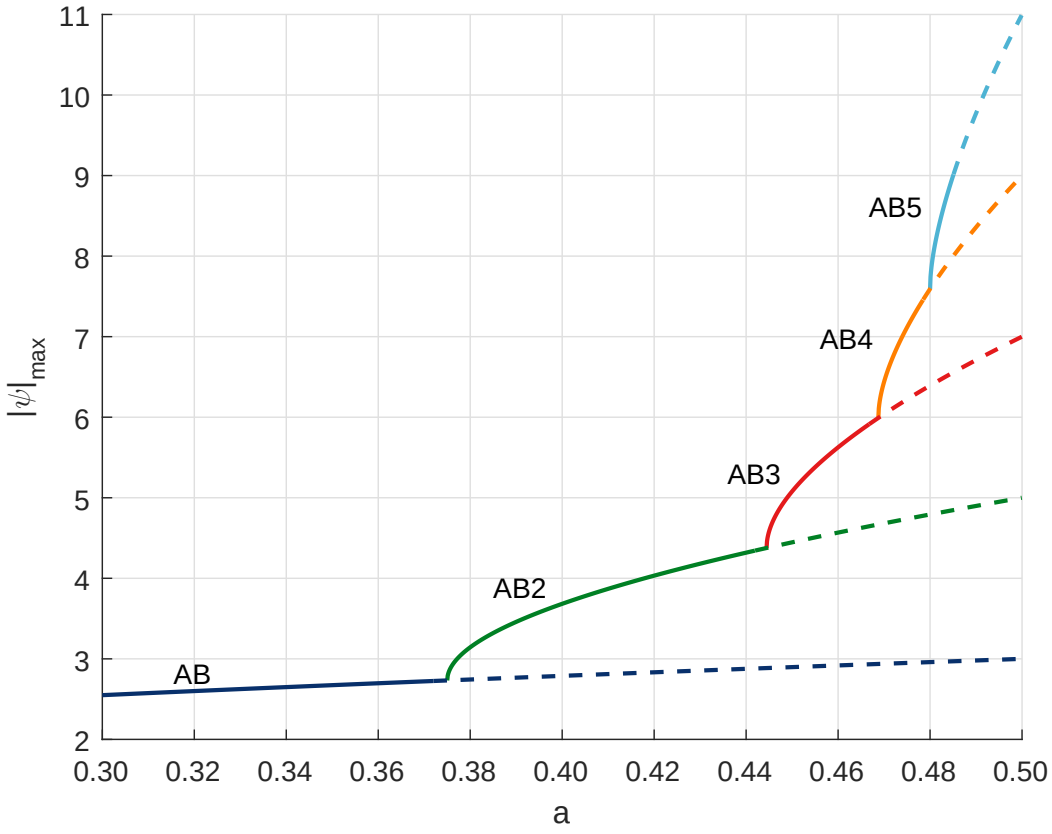

Fig. 3.4: Plot of the peak-height formula (2.1) for with $\nu_m = \sqrt{2a_m}$ for breathers on a constant background. It can be seen that the maximal intensity family (solid lines) is continuous. Dashed lines represent breathers which have the highest intensity within their period and order, but not within the period overall (since they are superseded by the solid lines of higher order breathers).

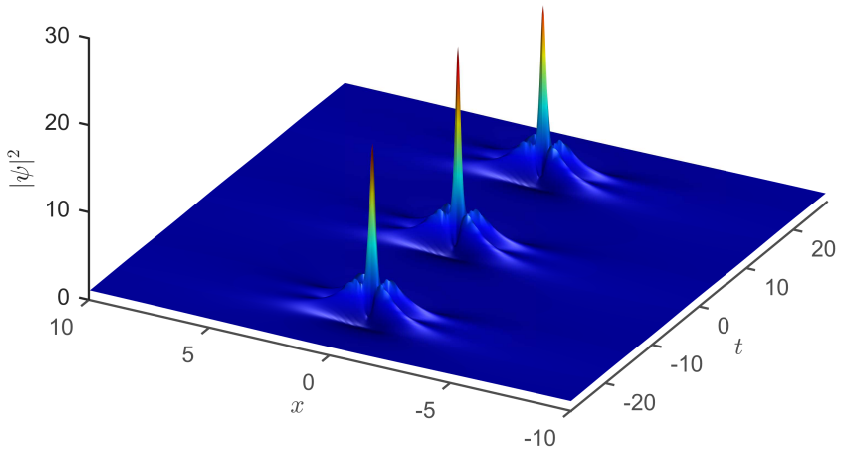

(a)

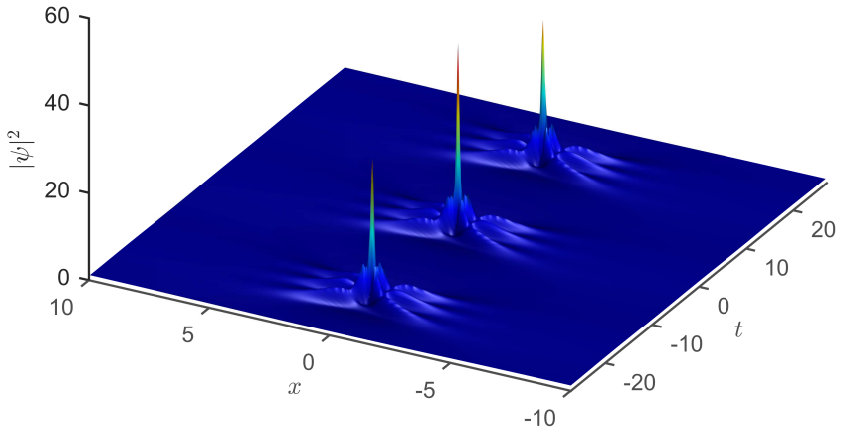

(b)

Fig. 3.5: Fully periodic higher order breathers. (a) second-order with $a_m = (0.485, 0.440)$ (b) third-order with $a_m = (0.485, 0.44, 0.365)$. Eq. (3.12) is used to obtain the higher values of a_m). The peak height formula predicts intensities of 24.48, 42.96 respectively, in line with the numerical DT results.

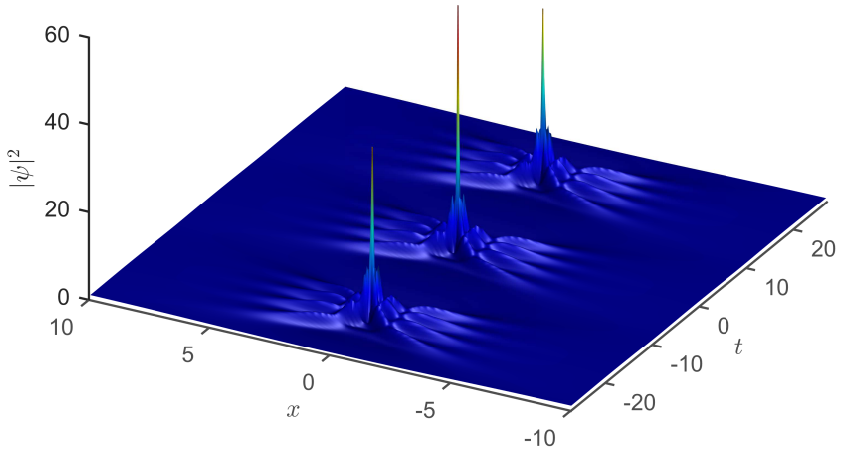

(a)

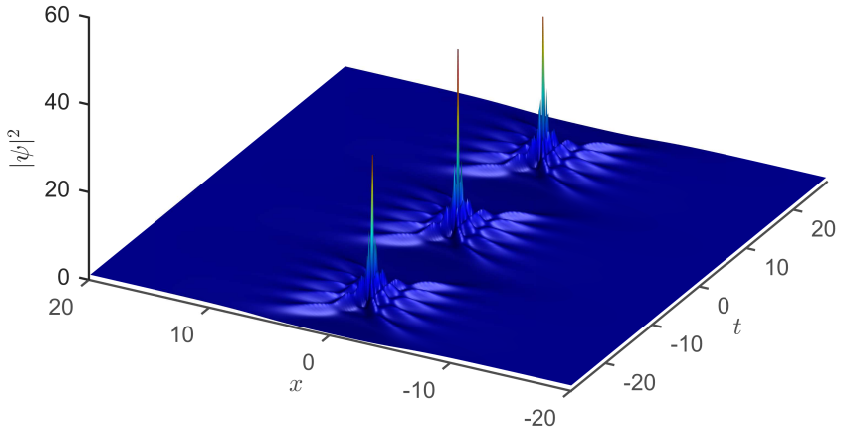

(b)

Fig. 3.6: Fully periodic higher order breathers. (a) fourth-order with $a_m = (0.485, 0.440, 0.365, 0.260)$ (b) fifth-order with $a_m = (0.485, 0.440, 0.365, 0.260, 0.125)$. Eq. (3.12) is used to obtain the higher values of a_j). The peak height formula predicts intensities of 63.95, 80.94 respectively, in line with the numerical DT results.

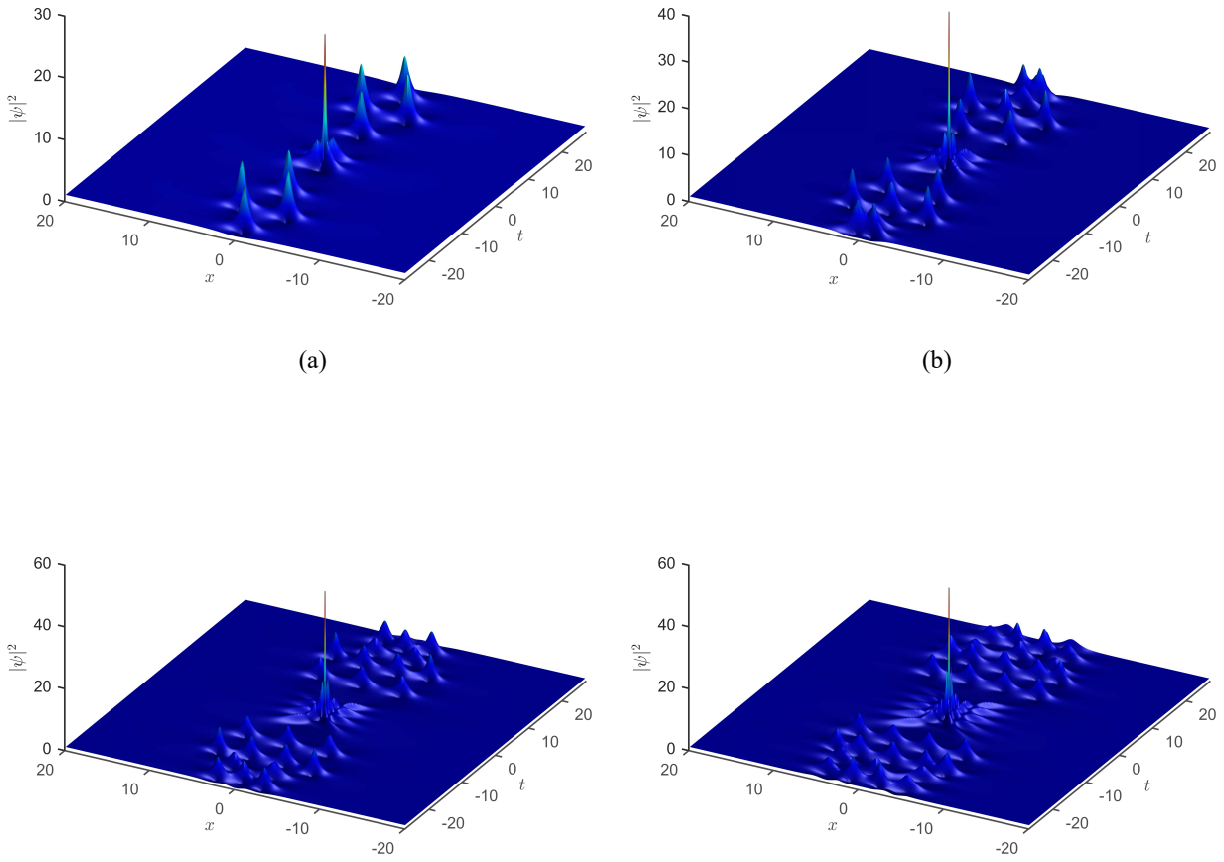

Fig. 3.7: Non-periodic higher order breathers. (a) second-order with $a = (0.485, 0.400)$ (b) third-order with $a = (0.485, 0.400, 0.330)$ (c) fourth-order with $a = (0.485, 0.400, 0.330, 0.250, 0.180)$ (d) fifth-order with $a = (0.485, 0.400, 0.330, 0.250, 0.180)$. The effect of slightly changing the higher-order a_m is drastic in comparison to Fig. 3.5 and Fig. 3.6 is drastic. The peak height formula predicts intensities of 22.64, 40.75, 60.80, 40.96 respectively, in line with the numerical DT results.

For the special set of a_m given by (3.12), in the $a_n^* < a < a_{n+1}^*$, there is a unique nth-order AB, and as proved in our work [41], it has maximal peak height. This is because it is a sum over all the available a_m's that produce commensurate values of κ. In regions below a_n^*, this n^{th}-order AB does not exist because at least one of the a_m's is negative (as seen in Fig. 3.3) and thus an invalid parameter for the DT.

To further illustrate this point, assume we pick $a = 0.45$. This a lies in the region $a_3^* < a < a_4^*$, and thus can produce a third order AB. For the sake of the argument, let's use it to produce a fully periodic AB2. One option would be to use $\kappa_2 = 2\kappa$, which gives $a_2 = 0.3$. Another option would be to use $\kappa_2 = 3\kappa$, which gives $a_2 = 0.05$. Both of these values of a_2, combined with $a = 0.45$, form periodic AB2. However, using the PHF (3.8), it is clear that the breathers with the set $a = (0.45, 0.36)$ (i.e. given by Eq. (3.12)) has a much higher intensity than that given by $a = (0.45, 0.05)$. Since these two values of a_2 are the only ones in this interval that can produce a fully periodic AB2, it is clear that the special set of parameters given by Eq. (3.12) gives the maximal intensity breathers within a given period. It should be noted that while breathers with degenerate eigenvalues have been studied [10, 43], they are actually aperiodic rogue waves as shown in [10] and thus are not relevant to our family. Moreover, they cannot be described by the inverse scattering transform (or the Darboux transformation) and require special treatment [10].

3. Breathers with Rational Ratios of κ

Additionally, one can study breathers with rational non-integer ratios of κ_m. In this case, we have the relation $\kappa_m = \frac{Q_m}{P_m}\kappa$, where $Q_m > P_m$ are integers and $\kappa \equiv \kappa_1$ as before. The relationship between the different a_m parameters is given by:

$$a_m = R_m^2\left(a - \frac{1}{2}\right) + \frac{1}{2}, \tag{3.14}$$

where $R_m \equiv \frac{Q_m}{P_m} \in \mathbb{Q}$ and $R_1 \equiv 1$. In this case, the periodic length is given by:

$$L = \text{LCM}(P_m)\frac{\pi}{\sqrt{1-2a}} \tag{3.15}$$

where $\text{LCM}(P_m)$ represents the lowest common multiple of all the denominators P_m (with $P_1 \equiv 1$). Note that if R_m is an integer as in 3.12, $\text{LCM}(P_m)$ evaluates to 1 and we retrieve our usual periodic length formula.

From Fig. 3.8, one can see that for the simplest case of AB2, the solution takes the form of an AB2 centered at $(0, 0)$, with $2(P_m - 1)$ AB1s, divided into 4 quadrants with $(P_m - 1)/2$ AB1s each. For higher order ABs, the structure becomes significantly more complicated with higher order breathers

present (e.g. AB2 in Fig. 3.8 (d)) as well as "smears" due to the nonlinear superposition of multiple breathers, but maintains the central ABn peak. Note that second order breathers with $R_m = (1, 3/2)$ have been produced experimentally in Ref. [15].

It is interesting to note that one can produce some interesting structures by adjusting the x and t shifts of these solutions, such as the Olympic rings and squiggly lines shown in Fig. 3.9.

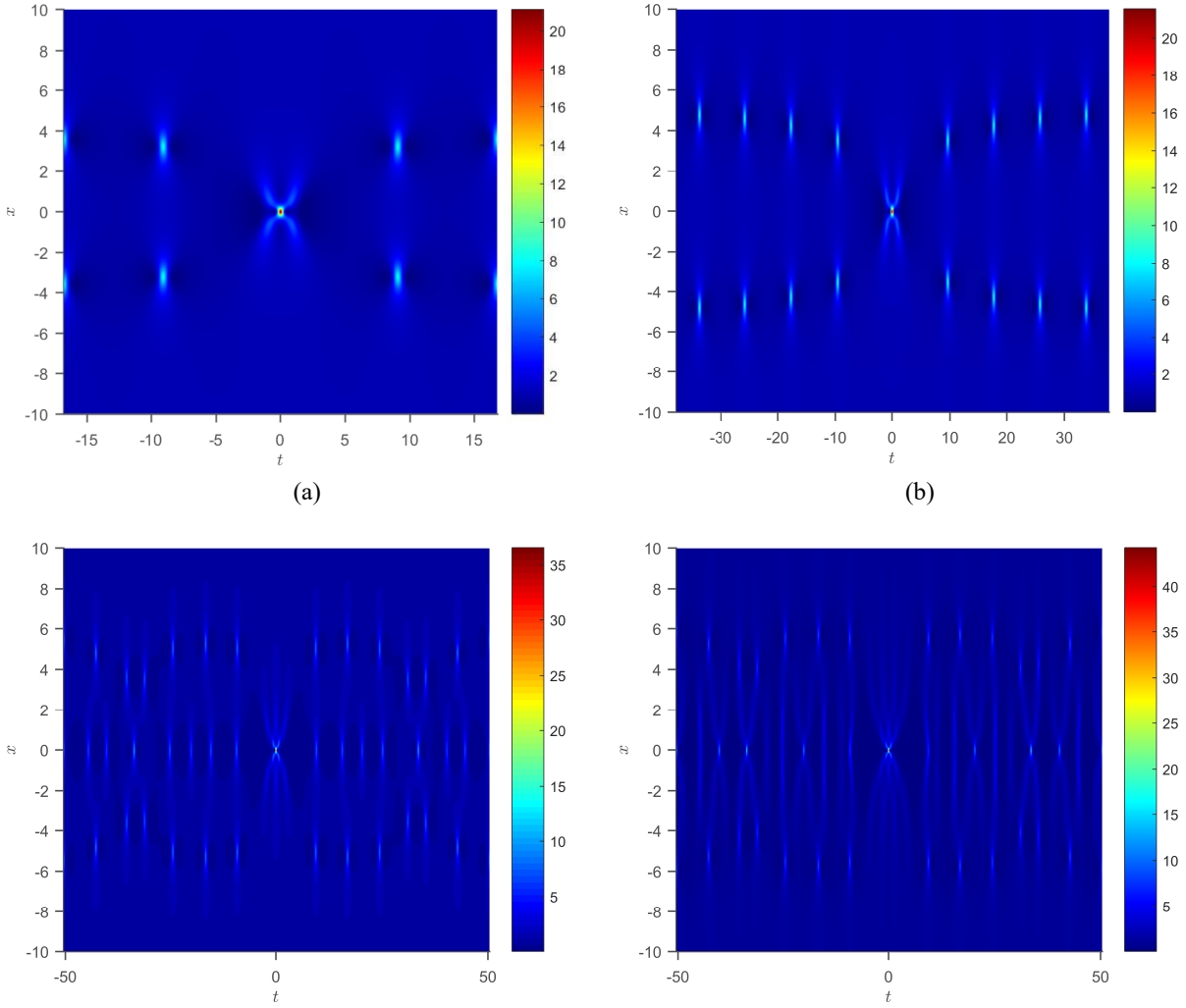

Fig. 3.8: Periodic Higher-order breathers with non-integer ratios of wavenumbers. All figures show 1 period and have $a = 0.43$ (a) AB2 R_m = (1,5/4), (b) AB2 with R_m = (1, 10/9) (c) AB3 with R_m = (1, 5/4, 5/3) (d) AB4 with R_m = (1, 5/4, 5/3, 5/2).

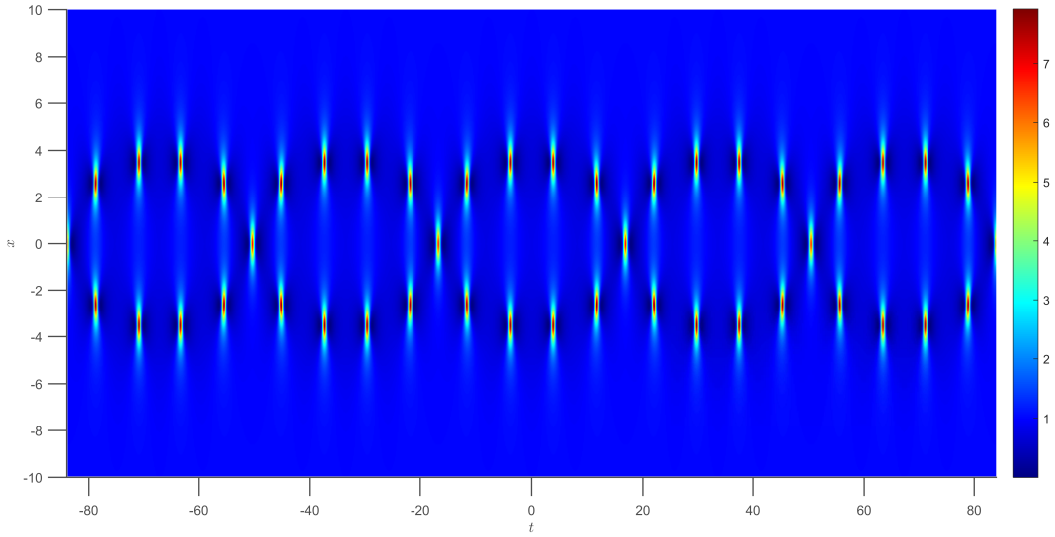

(a)

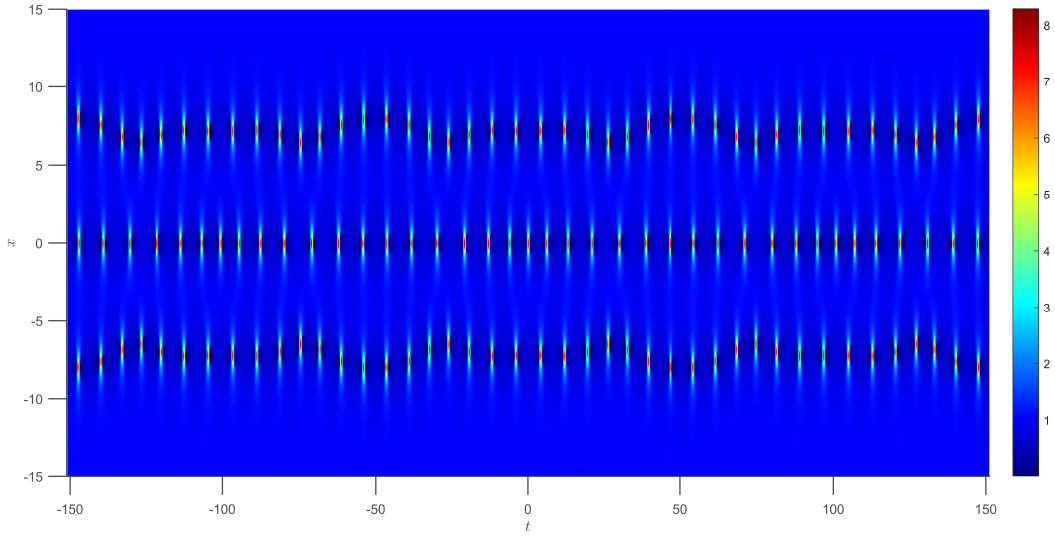

(b)

Fig. 3.9: (a) "Olympics rings" formed by a second order breather with $R_m = (1, 5/4)$, $a = 0.43$, $t_m = (L/2, 0)$ and $x_m = (0, 0)$, where L is the periodic length given by (3.15). Five periods are shown. (b) Squiggly lines formed by a third order breather with $R_m = (1, 5/4, 7/6)$, $a = 0.43$, $t_m = (L/2, 0, 0)$ and $x_m = (0, 0, 0)$. Three periods are shown.

CHAPTER IV

NUMERICAL GENERATION OF BREATHERS

Now that we have analytically demonstrated a family of maximal intensity, the next step is to find a method for numerically studying them so one can observe nonlinear effects such as modulation instability of the noise, something not observed in analytical solutions. Possible experimental applications will be discussed later in this chapter.

1. The Initial Conditions

Noting that an Akhmediev breather at $x = 0$ is symmetric about the line $t = 0$, and due to the properties of the NLSE, must remain so as time propagates [6, 11] . Therefore, the solution can be written as a cosine series [11]:

$$\psi(x,t) = A_0 + 2\sum_{m=1}^{\infty} A_m(t)\cos(m\kappa x) \tag{4.1}$$

where κ is the fundamental wavenumber as given in Chapter III. As shown in Ref. [9], for a breather with one unstable mode, all modes with $|m| > 1$ are locked to the A_1 mode, growing exponentially as $|A_m(x)| \sim |A_1(x)|^{|m|}$, leading to the so-called cascading instability. Therefore, at a sufficiently long distance x before the AB peak, all modes with $|m| > 1$ are much smaller in comparison to $A_1(x)$, and the initial wave function can be written as [9]:

$$\psi_0(t) = A_0 + 2A_1\cos(\kappa t), \tag{4.2}$$

with small A_1 and A_0 close to 1. Generalizing this result to an n^{th}-order AB (i.e. with at least n unstable modes), the wave function is of the form:

$$\psi(x,t) = A_0 + 2\sum_{m=1}^{n} A_m\cos(m\kappa t) \tag{4.3}$$

where all the A_m are generally complex.

2. Systematic Generation of Coefficients

In this section, we propose our method for *systematically* calculating all the coefficients $A_1, \ldots A_n$ needed to generate an n^{th} -order AB numerically. Pseudo-code for the algorithm is shown in Algorithm 1. Essentially, we generate a DT wavefunction over one period at some distance $x = X$ before the peak. This wavefunction is fit to a cosine series of the form (4.3). The phase of A_0 is subtracted from all the coefficients (noting that phase shifts does not change the solution [6]). This guarantees a real A_0.

Algorithm 1 Coefficient Generation

$n \leftarrow$ order of AB of interest
$a \leftarrow$ fundamental modulation parameter a
$X \leftarrow$ distance before peak to fit the breather
procedure GENCOEFF(a,n)
    $\kappa \leftarrow 2\sqrt{1-2a}$
    $L \leftarrow 2\pi/\kappa$
    $a \leftarrow$ array of a_m given by Eq. 3.12
    $\psi_{DT} \leftarrow$ DT wavefunction at $x = X$, $t = [-L/2, L/2)$, with parameters a and order n
    $B \leftarrow$ coefficients from fitting Ψ_{DT} to A[0] + $2\sum_{m=1}^{n}$ A[m] cos$(m\kappa t)$
    $\phi \leftarrow$ arg(B[0])
    for $k = 1 \rightarrow k = n$ **do**
        A[k] = A[k]/exp(iϕ) ▷ Subtract phase of A[0] to get a real A[0] in the end
    end for
    A[0] $\leftarrow$1
    for $k = 1 \rightarrow k = n$ **do**
        A[0] = A[0] - 2*Abs(A[k])^2 ▷ This is actually $A[0]^2$
    end for
    A[0] = sqrt(A[0])
    return A ▷ Final array of normalized coefficients
end procedure

Since the wavefunction needs (4.3) to be normalized as [9]:

$$\frac{1}{L}\int_0^L |\psi_0|^2 dt = A_0^2 + 2\sum_{m=1}^{n} |A_m|^2 = 1, \tag{4.4}$$

so we set $A_0 = \sqrt{1 - 2\sum_{m=1}^{n} |A_0|^2}$, and this concludes the systematic generation of the coefficients.

Figure 4.1 shows the results of using this algorithm to systematically generate second order breathers, and compares the results to the analytical form in both ordinary and Fourier space. In Fig. 4.1 (c,d), the algorithm is used with $X = -10$, i.e. the coefficients are generated by fitting the analytical breather 10 x units before the peak. It is seen that the coefficients are small, their modulus on the order of 10^{-4}. Moreover, the result looks exactly like the analytical breather, both in ordinary and Fourier space. Contrast this to Fig. 4.1 (e, f), where $X = -4$. The coefficients are much larger ($|A_m|$~10^{-2}), but the fit is not as good. This is not very clear in ordinary space, but the spectral signature clearly differs from the analytical one.

Figures 4.2 and 4.3 show systematically generated AB3 and AB4 respectively. The result is also very closely matched to the analytical breathers in both spaces.

3. Artificial Nonlinear Talbot Carpets

Additionally, one can use this method to generate nonlinear Talbot carpets numerically. This makes use of the modulation instability (MI) of these solutions, as discussed in [9, 11, 44]. In numerical [9, 45] and experimental studies [45, 46], noise also undergoes MI due to finite precision, leading to interesting recurrence.

The first step in generating such a carpet is to find an alternating AB recurrence. For example, with an AB1, one needs to find a coefficient A_1 that leads to an alternating pattern of ABs, with one peak centered at $t = 0$ and the next one centered at the borders of the box, *etc*. The easiest way to pick this coefficient is to select a purely imaginary value of A_1. Generating carpets of AB2 is much more challenging as it is very hard to find a recurring AB2, let alone an alternating one.

The next step is to select a periodic multiple in which to run the simulation, for example, 5 periodic boxes. In this case, the AB will be formed by the modes A_1, A_5, $A_{10} \ldots A_{5m}$. However, as seen in Fig. 4.4, the non-quintuplet modes, mere *noise*, grow exponentially from zero, completely ruining the carpet after just two iterations and eventually leading to chaotic behavior. This would not be observed on a computer with infinite precision.

The solution to this issue is to *forcefully* kill off those modes. This has to be done after every single step of the second order algorithm as shown in Listing A.2 in Appendix A. The result of using this

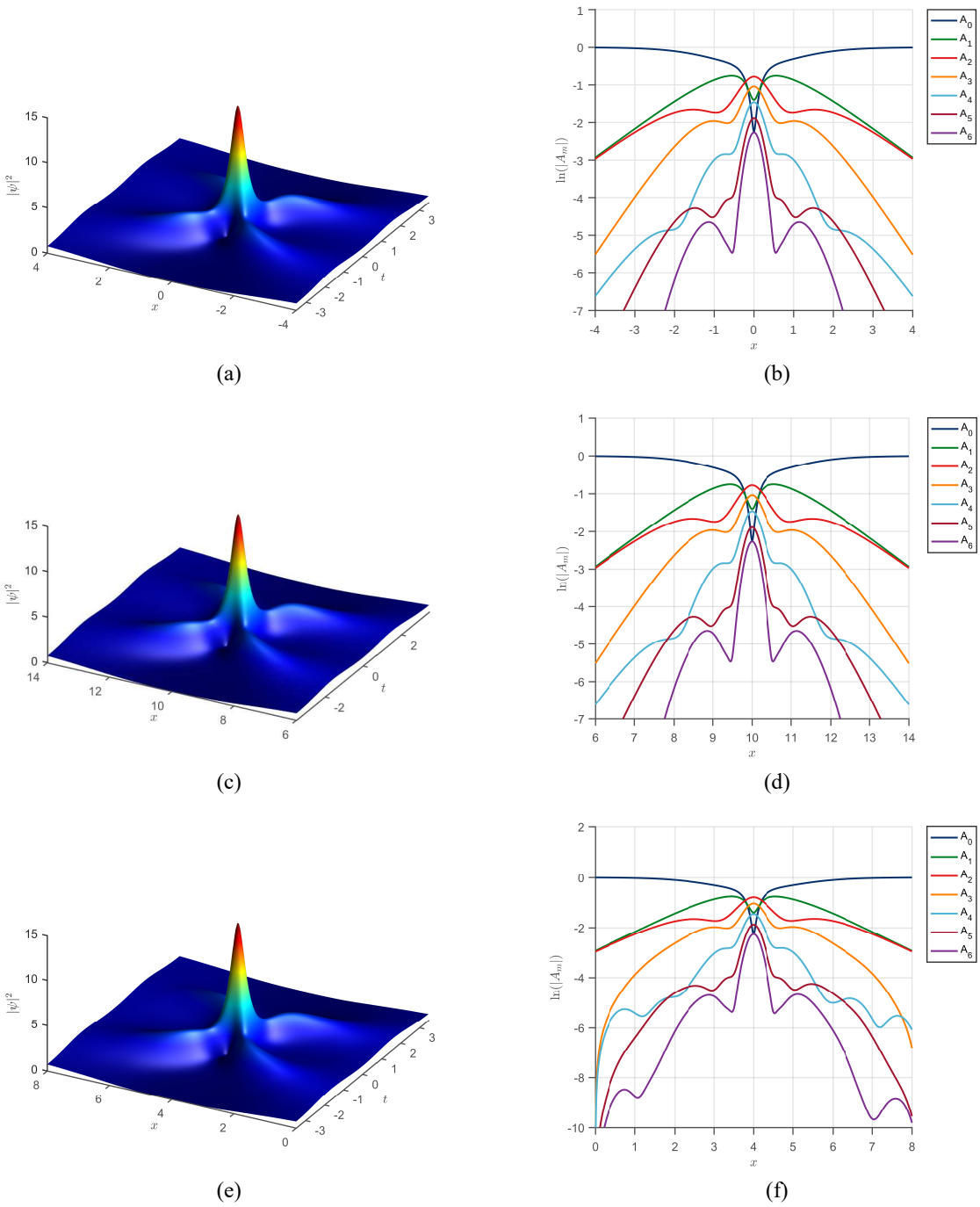

Fig. 4.1: Numerical and analytical second order breather with $a = 0.4$ (a) Analytical from the Darboux transformation, peak intensity is 13.567. (b) its spectrum (c) numerical solution with initial condition (4.3) with $A_1 = (2.0023 + 3.9986i) \times 10^{-4}$ and $A_2 = -(3.9996 + 1.9983i) \times 10^{-4}$, fit at $X = -10$ before the peak. Peak intensity is 13.567, as predicted by DT and PHF. (d) numerical spectrum. (e) numerical solution with $A_1 = (2.7 + 4.6i) \times 10^{-2}$, $A_2 = (4.7 - 2.1i) \times 10^{-2}$, fit at $X = -4$ before the peak. Peak intensity is 13.626, slightly higher than theory. (f) its spectrum. Both (c) and (e) use fourth-order symplectic integrators.

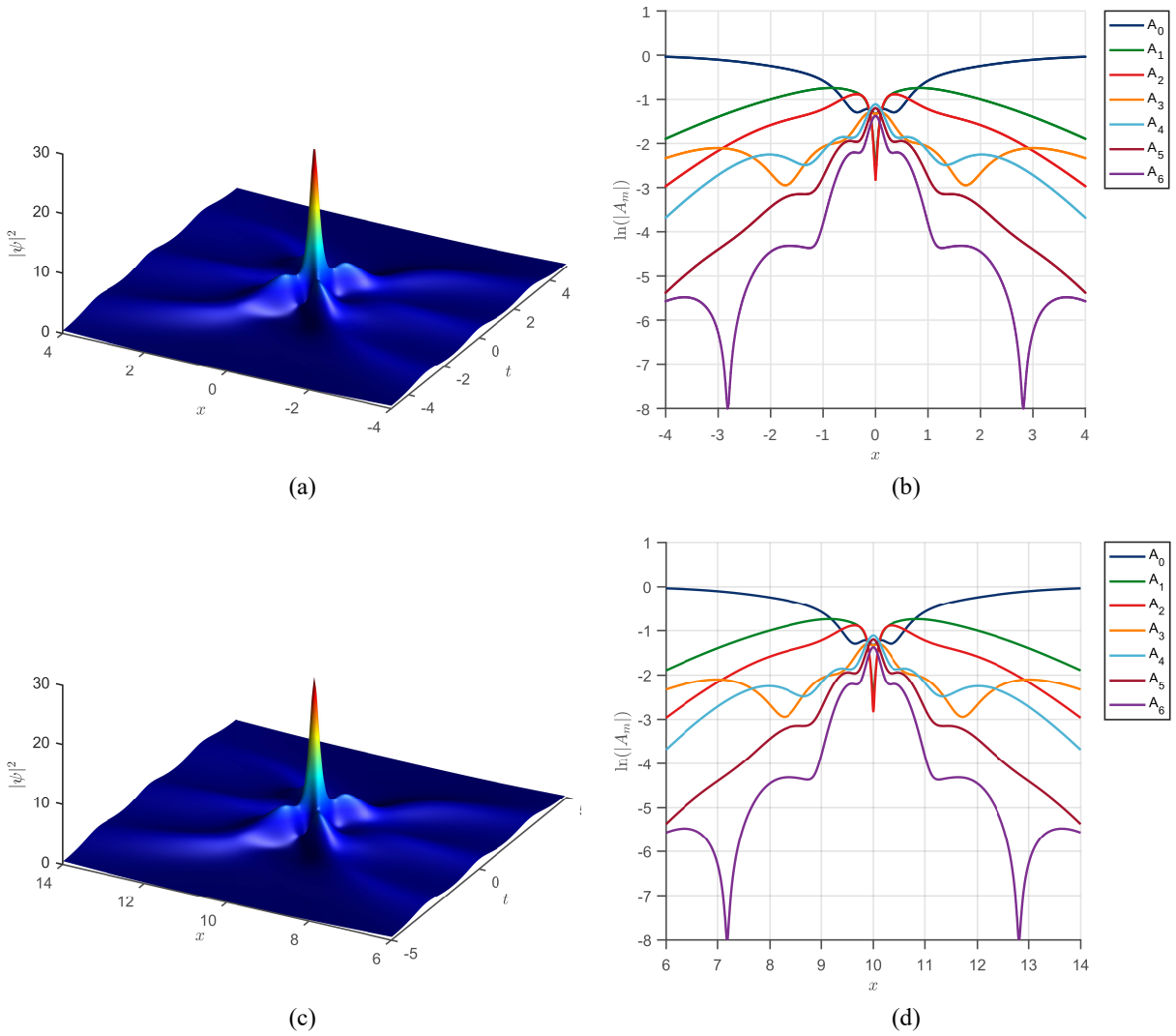

Fig. 4.2: Numerical and analytical third order breathers with $a = 0.45$ (a) Analytical from the Darboux transformation, peak intensity is 27.796, (b) its spectrum. (c) Numerical solution with initial condition (4.3) with $A_1 = (1.4005 + 4.1956i) \times 10^{-3}$, $A_2 = -(1.4780 + 1.3168i) \times 10^{-4}$ and $A_3 = (3.0815 + 1.0259i) \times 10^{-3}$ fit at $X = -10$ before the peak. Peak intensity is 13.567, as predicted by DT and PHF. (d) Its numerical spectrum.

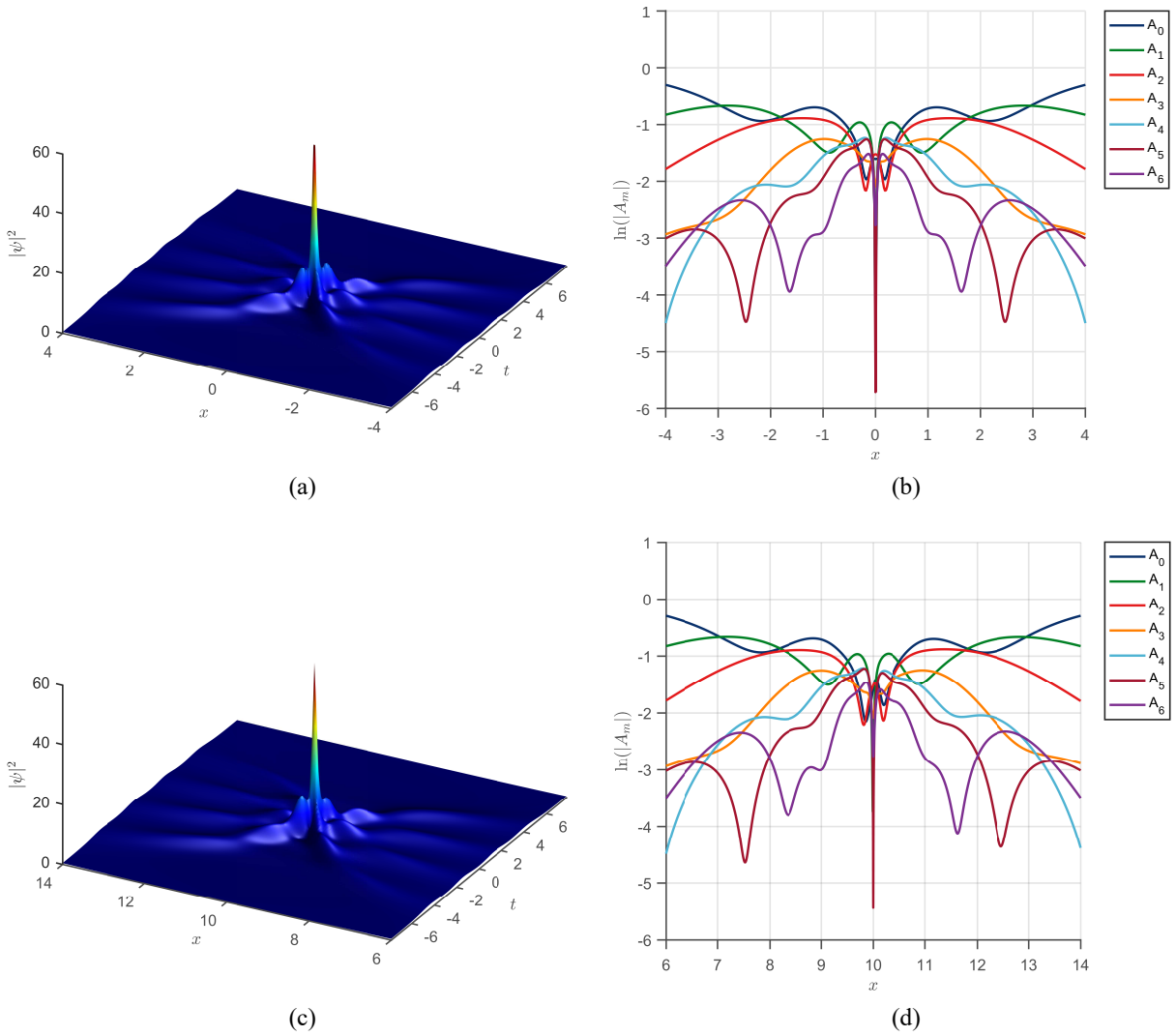

Fig. 4.3: Numerical and analytical fourth order breathers with $a = 0.48$ (a) Analytical from the Darboux transformation, peak intensity is 57.648, (b) its spectrum. (c) Numerical solution with initial condition 4.3 with $A_1 = (1.0407 + 4.9901i) \times 10^{-2}$, $A_2 = -(2.6818e - 03 + 2.6318i) \times 10^{-3}$, $A_3 = (6.0784 + 4.3164i) \times 10^{-4}$ and $A_4 = -(4.2588 + 2.5710i) \times 10^{-4}$ fit at $X = -10$ before the peak. Peak intensity is 56.936, slightly lower than DT and PHF. (d) numerical spectrum.

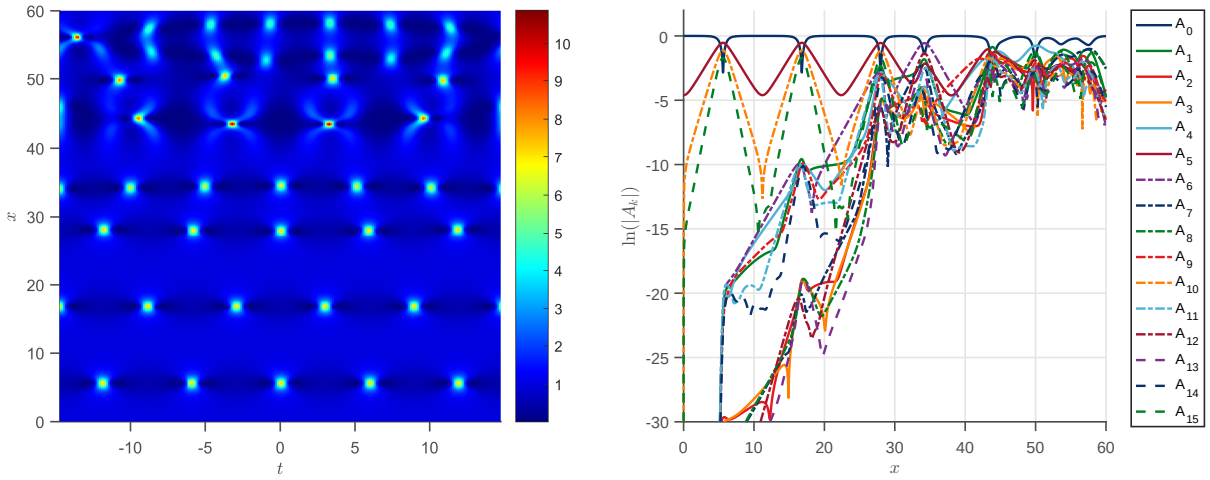

(a) (b)

Fig. 4.4: (a) a failed attempt at generating a nonlinear Talbot carpet due to the growing modes at $a = 0.36$ with $A_1 = 10^{-2}i$. The periodic length is set to 5, and thus, the A_{5k} modes are the ones responsible for forming the breathers. However, as seen in the spectrum (b), the noise of non-quintuplet modes grows exponentially from 0 until it eventually ruin the carpet, leading to the chaotic behavior seen later in (a).

method to generate these *artificial* carpets is shown in Fig. 4.5 for carpets of AB1, AB2 and a mix of both.

4. Experimental Studies of Higher Order ABs in Optical Fibers

It is known that the nonlinear Schrodinger equation models light pulses in nonlinear fibers relatively adequately [4], and first and second order breathers have already been observed through trial and error with the wave function coefficients or exact initial conditions [15, 20, 47]. However, using exact initial conditions is inconvenient and not easily done in optics [15], and using cosine modulation (4.3) is cumbersome because it requires trial and error to obtain the correct A_m required to "collide" the lower order breathers to form higher order ones. However, our results and as shown in this chapter strongly suggest that it is possible to pick the coefficients A_m properly using our method to collide the breathers accurately, without the need for excessive trial and error.

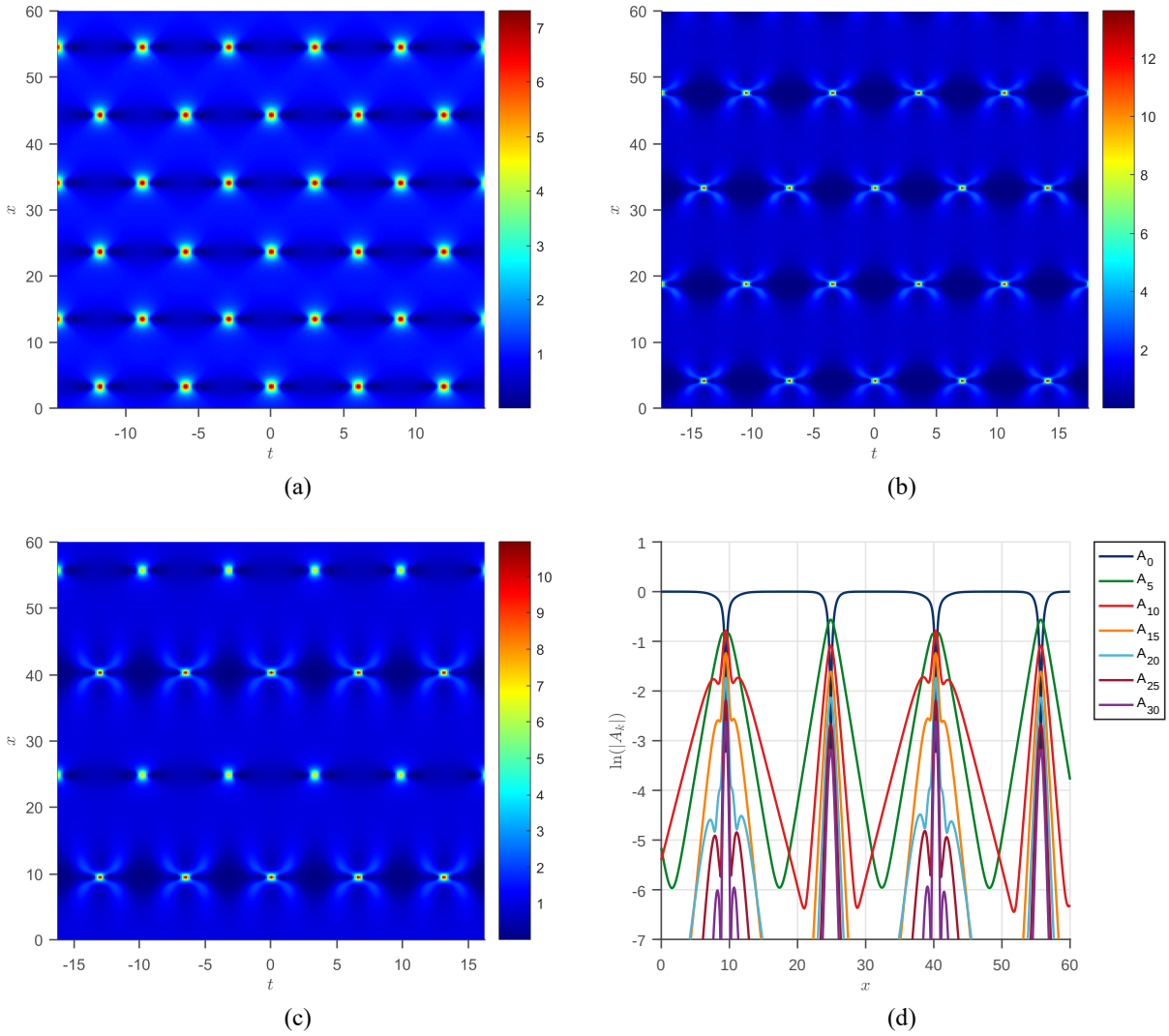

Fig. 4.5: Nonlinear Talbot carpets of breathers. (a) AB1 carpet with $a = 0.36$ with $A_1 = (2.7 + 4.6i) \times 10^{-2}$. Peak intensity is 7.33 (7.27) (b) AB2 carpet with $a = 0.4$, $A_1 = (2.7 + 4.6i) \times 10^{-2}$, $A_2 = (4.7 - 2.1i) \times 10^{-2}$. Peak intensity is 13.62 (13.56). (d) Carpet with alternating AB2 and AB1 at $a = 0.38476505$ and $A_1 = (-2.5107 + 5.1832i) \times 10^{-3}$, $A_2 = -(4.3133 + 1.2877i) \times 10^{-3}$. (d) Its spectrum, clearly showing alternating AB2 and AB1 signatures. All figures use fourth order symplectic integrators.

CHAPTER V

MAXIMAL INTENSITY BREATHERS ON AN ELLIPTIC DN BACKGROUND

Another family of NLSE solutions is given by the seed

$$\psi_0 = \text{dn}(t - t_0, k) e^{i(x-x_0)(1-\frac{k^2}{2})}, \tag{5.1}$$

where t_0 and x_0 are t and x shifts as before, k is the elliptic modulus (NOT the elliptic parameter, k^2). Transforming the Lax pair generating functions r_{1m} and s_{1m} into the form:

$$\begin{aligned} r_{1m}(x,t) &= a_{1m}(x,t) e^{\frac{ix}{4}(k^2-2)} \\ s_{1m}(x,t) &= a_{1m}(x,t) e^{-\frac{ix}{4}(k^2-2)} \end{aligned} \tag{5.2}$$

then substituting in the Lax Pair equation (1.6), one gets [12]:

$$\begin{aligned} a_t &= i\lambda a + ib\text{dn}(t,k), \\ b_t &= -i\lambda b + ia\text{dn}(t,g), \\ a_x &= \frac{1}{2}ia\left(2\lambda^2 + k^2\left(\text{sn}^2(t,k) - \frac{1}{2}\right)\right) + b\left(i\lambda\text{dn}(t,k) - \frac{k^2}{2}\text{sn}(t,k)\text{cn}(t,k)\right), \\ b_x &= -\frac{1}{2}ib\left(2\lambda^2 + k^2\left(\text{sn}^2(t,k) - \frac{1}{2}\right)\right) + a\left(i\lambda\text{dn}(t,k) + \frac{k^2}{2}\text{sn}(t,k)\text{cn}(t,k)\right). \end{aligned} \tag{5.3}$$

However, as noted in [12], the four coupled first order differential equations (5.3) cannot be solved analytically. However, one can solve for the profiles and derivatives at $t = 0$, given by [12]:

$$\begin{aligned} a_{1m}|_{t=0} &= Ae^{i(\chi_m + \kappa_m\lambda_m(x-x_m))} - Be^{-i(\chi_m+\kappa_m\lambda_m(x-x_m))}, \\ b_{1m}|_{t=0} &= Ae^{i(-\chi_m + \kappa_m\lambda_m(x-x_m))} + Be^{-i(-\chi_m+\kappa_m\lambda_m(x-x_m))}, \\ a_{1m,t}|_{t=0} &= i(\lambda_m a_{1m}|_{t=0} + b_{1m}|_{t=0}), \\ b_{1m,t}|_{t=0} &= -i(\lambda_m b_{1m}|_{t=0} - a_{1m}|_{t=0}), \end{aligned} \tag{5.4}$$

where

$$\kappa_m = \sqrt{\left(\lambda_m - \frac{k^2}{4\lambda_m}\right)^2 + 1} \tag{5.5}$$

is half the wavenumber of the m^{th} constituent breather (note that we previously used κ_m for the full wavenumber in the case of breathers on a constant background, this is common in the literature). $\chi_m = \arccos(\kappa_m)/2$ is the background dependent phase and A and B are two phase constants. The equations (5.4) can then be evolved in x using a suitable numerical method, such as Runge-Kutta methods. Since it is not possible to write down analytical solutions for this background, the Darboux transformation has to rely on numerical integration and thus introduces an additional, if minor, numerical error. Calculating DT solutions on a large grid could also be computationally expensive, depending on the numerical method selected.

However, one can still check the condition (2.3) to see whether the peak height formula (2.1) is obeyed. At $x = t = 0$ and $t_m = x_m = 0$ for all m, the first two equations in (5.4) reduce to:

$$\begin{aligned} a_{1m}|_{x=t=0} &= Ae^{i\chi_m} - Be^{-i\chi_m}, \\ a_{1m}|_{x=t=0} &= Ae^{-i\chi_m} + Be^{i\chi_m}. \end{aligned} \tag{5.6}$$

However, noting that the choice of phase constants $A = \exp(-i\pi/4) = B^*$ is universal in the literature (to center the breathers at the origin) [12, 27, 48], (5.6) further reduces to

$$\begin{aligned} r_{1m}(0,0) = a_{1m}(0,0) &= e^{i(\chi_m - \frac{\pi}{4})} - e^{-i(\chi_m - \frac{\pi}{4})} = 2i\sin(\chi_m - \frac{\pi}{4}) = -i\sqrt{2}(\cos\chi_m - \sin\chi_m), \\ s_{1m}(0,0) = b_{1m}(0,0) &= e^{-i(\chi_m + \frac{\pi}{4})} + e^{i(\chi_m + \frac{\pi}{4})} = 2\cos(\chi_m + \frac{\pi}{4}) = \sqrt{2}(\cos\chi_m - \sin\chi_m). \end{aligned} \tag{5.7}$$

or equivalently, $s_{1m}(0,0) = ir_{1m}(0,0)$, (i.e. (2.3) with $\phi = \pi/2$) and thus this family of solutions also obeys the PHF (2.1). Since $\psi_0(0,0) = 1$, the PHF reduces to:

$$\psi_n(0,0) = 1 + 2\sum_{m=1}^{n} \nu_m \tag{5.8}$$

1. The Fundamental Periodicity Condition

Consider a breather of order n on a dnoidal background. The m^{th} component is characterized by the half-wavenumber, assuming purely imaginary eigenvalues $\lambda_m = i\nu_m$

$$\kappa_m = \sqrt{\left(\lambda_m - \frac{k^2}{4\lambda_m}\right)^2 + 1} = \sqrt{-\frac{k^4}{16\nu_m^2} - \frac{k^2}{2} - \nu_m^2 + 1} \tag{5.9}$$

The "fundamental" periodicity condition arises from the fact that κ_m is not real for all combinations of parameters $(k, \nu_1, \nu_2, ...\nu_M)$. The expression under the root in (5.9) must be positive to yield a real value of κ_m.

$$-\frac{k^4}{16\nu_m^2} - \frac{k^2}{2} - \nu_m^2 + 1 > 0 \tag{5.10}$$

Consequently, the range where k is valid is given by:

$$0 \leq k < 2\sqrt{(1-\nu_m)\,\nu_m} \tag{5.11}$$

A plot of the first periodicity condition is shown in Fig. 5.1.

2. Matching the Background to the Breathers

As shown in Fig. 5.3, if one just picks arbitrary values of ν for a given k, the resulting breather is not periodic, in contrast to AB1s on a constant background which are always periodic. This is because the peaks of the breathers do not properly align with the peaks of the elliptic background, and consequently, one needs to match the period of the AB to the background. The period of the background is given by:

$$2K(k) = 2\int_0^{\frac{\pi}{2}} \frac{d\theta}{\sqrt{1 - k^2\sin^2\theta}} \tag{5.12}$$

where $K(k)$ is the complete elliptic integral of the first kind.

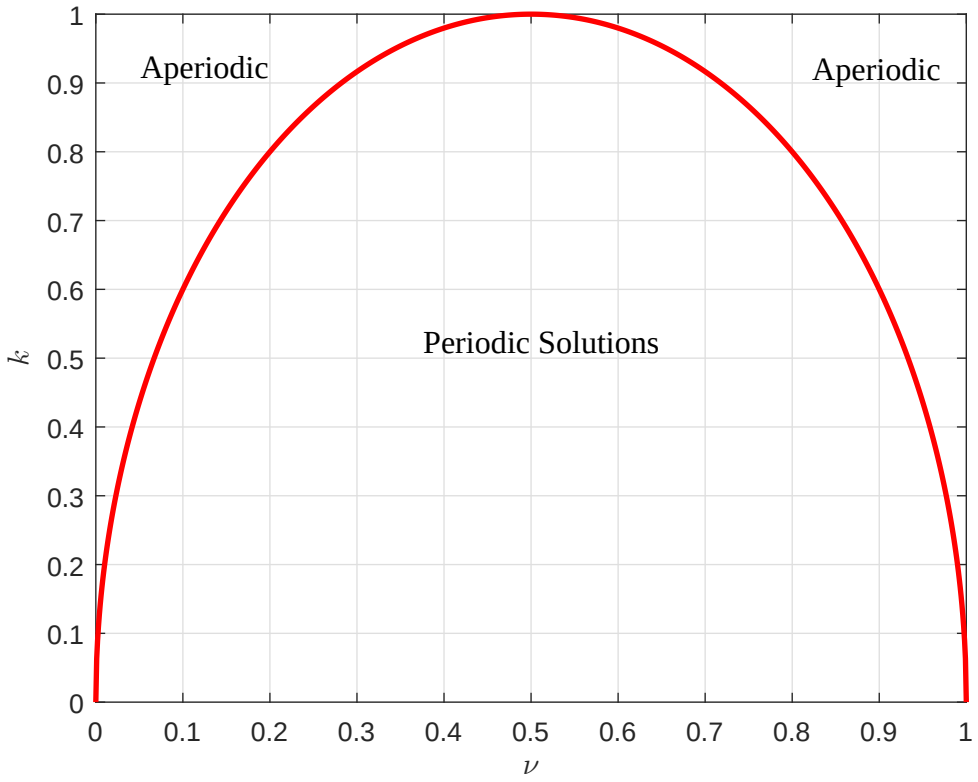

Fig. 5.1: Fundamental periodicity condition for breathers on a dnoidal background. Values of (ν, k) within the red parabola give periodic solutions.

It is now convenient to solve for ν in terms of κ. Starting from (5.9), one obtains:

$$\nu = \frac{1}{2}\sqrt{-2\kappa^2 + 2\sqrt{(\kappa^2-1)\left(\kappa^2+k^2-1\right)} - k^2 + 2} \tag{5.13}$$

This can be rewritten in the form:

$$\frac{1}{2}\sqrt{(\kappa')^2 + 2\sqrt{(\kappa')^2 D^2} + D^2} \tag{5.14}$$

with $\kappa' = \sqrt{1-\kappa^2}, D = \sqrt{(\kappa')^2 - k^2}$. From the Benjamin-Feir instability [49] or the Bogoliubov spectrum [9], $0 < 2\kappa < 2 \implies 0 < \kappa < 1$. Thus $\kappa' \in \mathbb{R}$, and it can be shown that $\kappa(k) > k \, \forall k < 2\sqrt{(1-\nu_m)\,\nu_m}$ from the fundamental periodicity condition. Consequently, one can rewrite (5.13) as:

$$\nu = \frac{1}{2}\left(\kappa' + \sqrt{(\kappa')^2 - k^2}\right) \tag{5.15}$$

Returning to the background, matching the period of the background (5.12) to the already-matched breathers requires:

$$\frac{\pi}{\kappa} = 2qK(k) \Rightarrow \kappa = \frac{\pi}{2qK(k)} \tag{5.16}$$

where $L = \pi/\kappa$ is the period of the breathers and q is some small integer. Substituting in (5.15), one can calculate ν at a specific k that gives a matched breather. It is possible to invert (5.16) numerically, so that one can calculate an elliptic modulus k given some modulation parameter ν. A plot of Eq. (5.16) is shown in Fig. 5.2, and a fully periodic AB1 on a dn background is shown in Fig. 5.3(b).

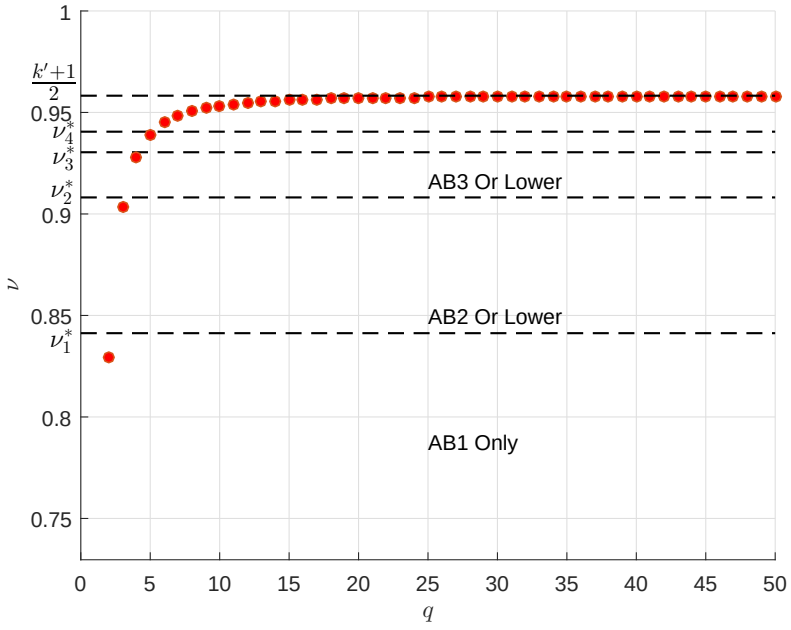

Fig. 5.2: Plot of Eq. (5.16) for multiple valyes of q. The horizontal dashed lines represent the lower limits of ν, ν_m^*, needed to generate a breather of order m (Eq. (5.25)), which will be discussed in the next section. As q gets larger, ν approaches $(k'+1)/2$ as will also be shown in the next section.

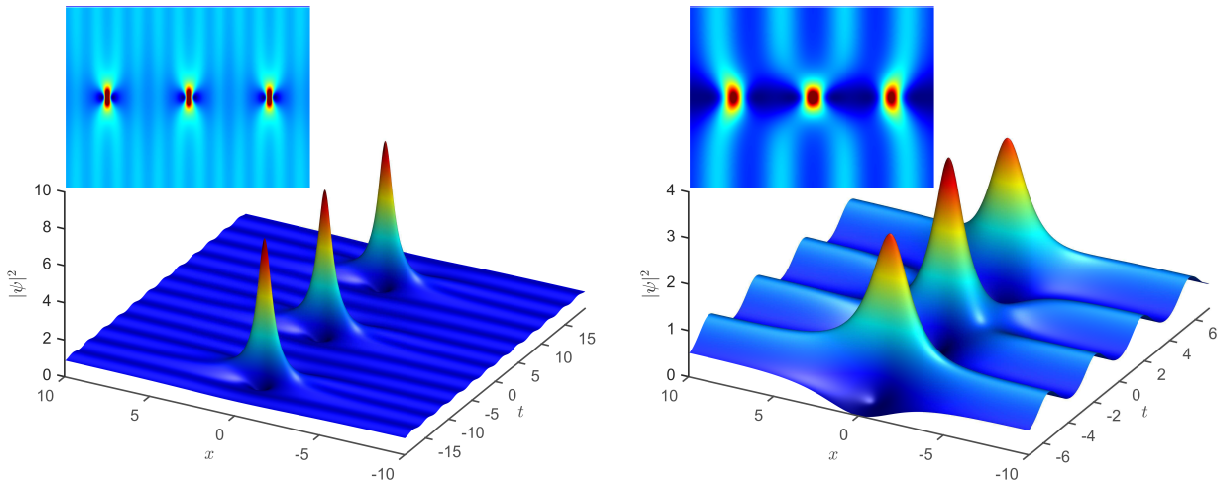

(a) (b)

Fig. 5.3: (a) Three periods of a first order AB *unmatched* to the dn background with $k^2 = 1/2$ and $\nu = 0.5$ (b) three periods of a first order AB matched to a dn background with $k^2 = 1/9$ and $\nu \approx 0.9405$ (q = 4 from (5.16)). Inset: top view with height lowered to show matching to background

3. Matching the Constituent Breather Periods

The second condition is similar to the case of breathers on a constant background, namely, one needs to match the periods of the constituent breathers forming the final higher-order structure. However, in this case, the equations are more complicated. To match all such periods, one needs wavenumbers κ_m such that:

$$\kappa_m = m\kappa\,, \tag{5.17}$$

where $\kappa \equiv \kappa_1$, and m is an integer. In full form, this equation reads:

$$m\sqrt{-\frac{k^4}{16\nu^2} - \frac{k^2}{2} - \nu^2 + 1} = \sqrt{-\frac{k^4}{16\nu_m^2} - \frac{k^2}{2} - \nu_m^2 + 1} \tag{5.18}$$

This equation has 4 solutions, 2 of which are neglected as they are negative. The other two solutions are:

$$\nu_m = \frac{\sqrt{G^2 \pm \sqrt{G^4 - 64k^4\nu^4}}}{4\sqrt{2}\nu}\,, \tag{5.19}$$

where

$$G = \sqrt{k^4 m^2 + 8\left(k^2 - 2\right)\left(m^2 - 1\right)\nu^2 + 16 m^2 \nu^4} \tag{5.20}$$

and $\nu \equiv \nu_1$. The solution with the minus sign does not give a maximal intensity family, and thus the positive root is selected. A plot of the solution for multiple values of m is shown in Fig. 5.4.

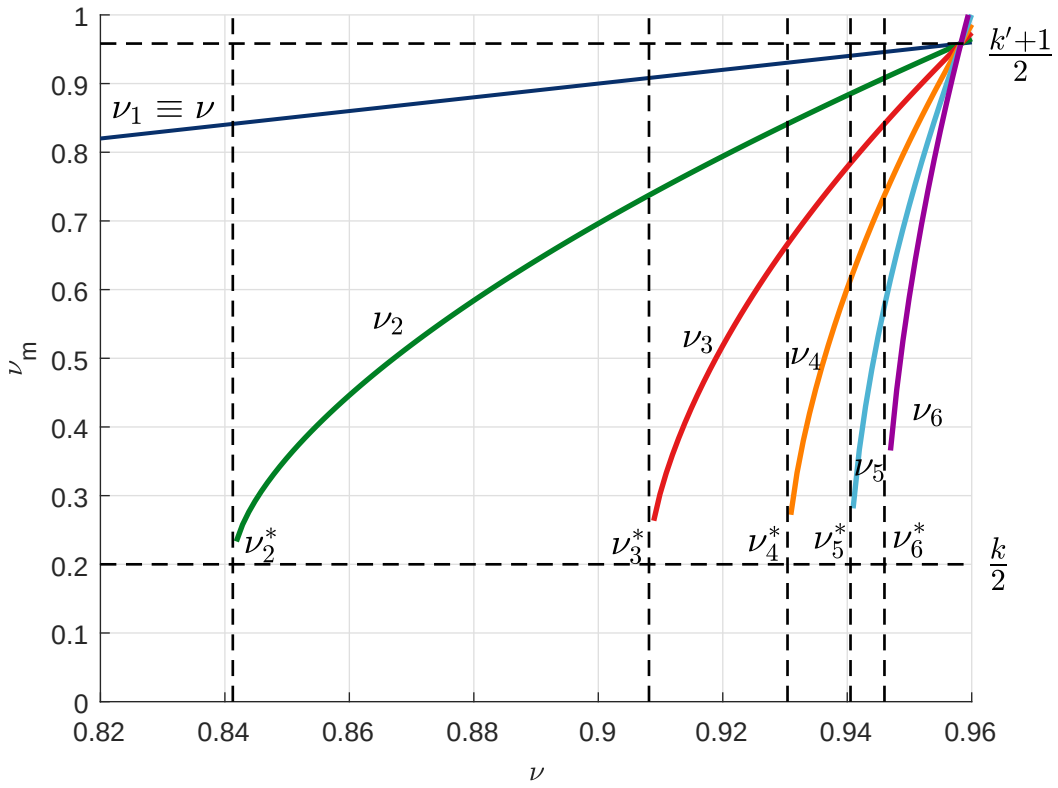

Fig. 5.4: Plot of the modulation parameters v_m as a function of m as given by (5.19) and their limits at k = 0.4. The dashed vertical lines represent the lower limit for an m^{th} order breather v_m^*, and the horizontal lines give the upper and lower limit on ν_m. Note that the lines at larger m appear to start higher than the $\nu_m = k/2$ line, this is merely because they have infinite slope near ν_m^* and thus cannot be plotted properly.

The next problem to tackle is finding the ranges where these curves are valid. All ν_m curves must meet at some point in the $\nu\nu_m$-plane ($(1,1)$ for breathers on a constant background). Consequently, this point is independent of m, so one can set $\nu_1 = \nu_2$ and solve for ν:

$$\nu_{\text{upper}} = \frac{k'}{2} + \frac{1}{2} \tag{5.21}$$

where $k' = \sqrt{1-k^2}$ is the complementary elliptic modulus. Thus, the two curves meet at the upper limit point in the $\nu\nu_m$-plane:

$$U = \left(\frac{k'}{2} + \frac{1}{2}, \frac{k'}{2} + \frac{1}{2}\right) \tag{5.22}$$

The next step is finding the lower point where the curves meet in the plane. From the breathers on a constant background case, we know that for a maximal intensity breather of order m to form, the fundamental eigenvalue $\nu \equiv \nu_1$ must be greater than some cut off ν_m^*. Essentially, one needs to find

$$\{\nu_m^* : \nu_m \in \mathbb{C}\, \forall \nu_m < \nu_m^*\} \tag{5.23}$$

Equation (5.19) with the positive root only returns complex values when the expression under the inner square root is negative. Consequently, one needs to solve:

$$G(\nu_m^*, \nu, k)^4 - 64k^4\nu^4 = 0 \tag{5.24}$$

This gives

$$\nu_m^* = \frac{\sqrt{2F+H}}{2m}\,, \tag{5.25}$$

where

$$F = \sqrt{(m^2-1)\left(k'\right)^2\left(m^2-\left(k'\right)^2\right)}\,,\; H = m^2\left(\left(k'\right)^2+1\right) - 2\left(k'\right)^2 \tag{5.26}$$

Substituting (5.25) into (5.19) to find the y-axis value of the minimum, one obtains the remarkable result of $k/2$, not 0. Referring back to the PHF (5.8), this means that when transitioning from an ABn

to an AB(n+1), the peak would instantly jump by $2(k/2) = k$ and would not just increase smoothly as one might expect. This can be seen clearly in Fig. 5.5. Contrast this to Fig. 3.4 for maximal intensity breathers on a constant background, where the peak heights are clearly continuous.

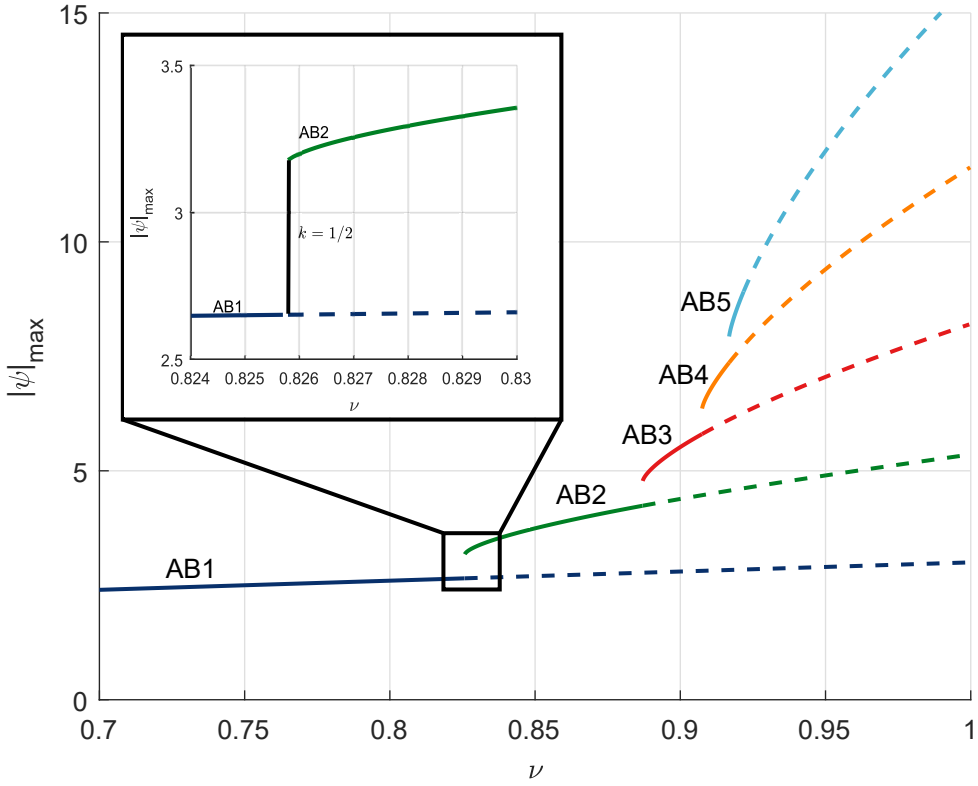

Fig. 5.5: Plot of the peak height formula (2.1) using the modulation parameters as given in (5.19). The insert shows a zoomed in version of the area between the peak heights of AB1 and AB2, with a gap of $k = 1/2$, making this family discontinuous. Note that the curves looks different from the constant background case (Fig. 3.4) since here they are plotted as a function of ν, not a.

Consequently, each curve ν_m has a path in the $\nu\nu_m$-plane that starts from the point:

$$L_m = (\nu_m^*, \frac{k}{2}) \tag{5.27}$$

and ends at the point U given by (5.22).

Figure 5.3 contrasts matched and unmatched first order breathers. It is clear that selecting a proper ν leads to a truly periodic structure (at least within the first few periods due to numerical errors accumulating). However, in case of an unmatched breather, the periodicity is completely destroyed.

Figure 5.6 shows matched and unmatched second and third order breathers. The effect of not matching the two components as well as the background is drastically clear, with only one major peak forming and the others completely vanishing. This could possibly serve as a more accurate model of rogue waves in contrast to the conventional model of breathers on a constant background with an infinite period [4].

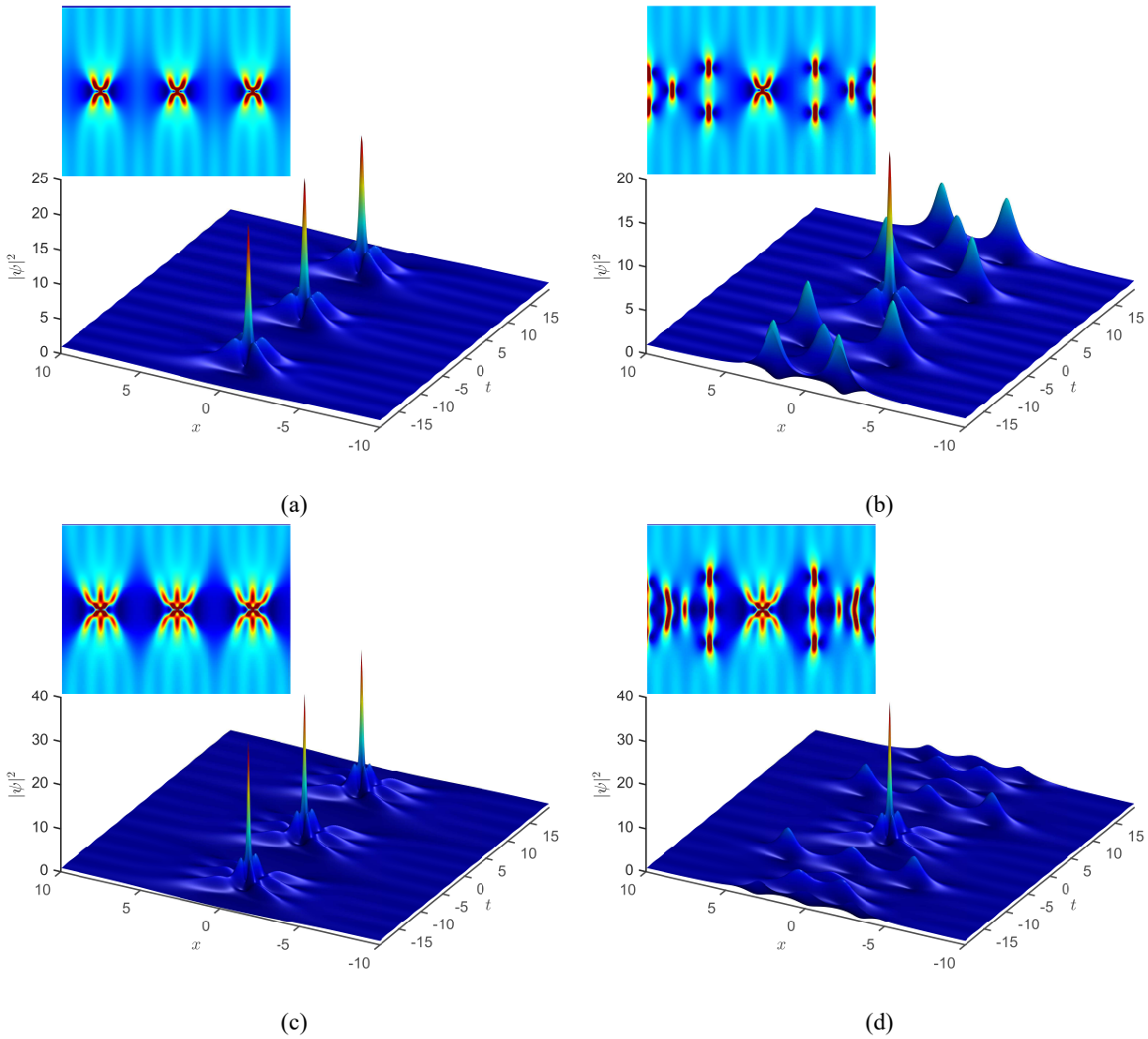

Fig. 5.6: Matched and unmatched higher order breathers on a dn background with $k^2 = 1/9$. (a) matched second order breather with $\nu \approx (0.9405, 0.8411)$, (b) unmatched second order AB with $\nu = (0.91, 0.81)$ (c) matched third order breather with $\nu \approx (0.9405, 0.8411, 0.6419)$. (d) unmatched third order AB with $k^2 = 1/9$ with $\nu = (0.91, 0.81, 0.61)$. Inset: top view with height lowered to show matching to background.

CHAPTER VI

CONCLUDING SUMMARY

In chapter II of this work, we presented a new analytical result, the peak-height formula:

$$\psi_n(0,0) = \psi_0(0,0) + 2\sum_{m=1}^{n} \nu_m, \tag{6.1}$$

and proved it using the Darboux transformation for background (or seed) solutions of the NLSE. This provides a simple check on numerical solutions of extended nonlinear Schrödinger equations.

Additionally, in chapter III, a family of fully periodic breathers of the cubic nonlinear Schrodinger equation on a constant background was derived. This family is characterized by modulation parameters that obey the relation:

$$a_m = m^2\left(a - \frac{1}{2}\right) + \frac{1}{2}, \tag{6.2}$$

which guarantees that the periods of the individual constituent breathers are commensurate with each other. We proved that this family has maximal intensity for a given period. This chapter also presented breathers with rational ratios of periods.

Moreover, in Chapter IV, we presented a *systematic* method for generating the coefficients of the initial condition:

$$\psi(x,t) = A_0 + 2\sum_{m=1}^{n} A_m \cos(m\kappa t), \tag{6.3}$$

as shown in Algorithm 1. This could possible be used by experimentalists to generate the initial wavefunctions needed to study these breathers experimentally in fibers. This chapter also presented "artificial" nonlinear Talbot carpets generated using this method.

Lastly, Chapter V presented a second maximal intensity family, but on an elliptic background. This family's eigenvalues follow the relation:

$$\nu_m = \frac{\sqrt{G^2 + \sqrt{G^4 - 64k^4\nu^4}}}{4\sqrt{2}\nu}\,, \tag{6.4}$$

where

$$G = \sqrt{k^4m^2 + 8\left(k^2 - 2\right)\left(m^2 - 1\right)\nu^2 + 16m^2\nu^4} \tag{6.5}$$

and reduces to the family in Chapter III when $k = 0$. Moreover, the background's period needs to be matched with the breathers so that:

$$\kappa = \frac{\pi}{2qK(k)} \tag{6.6}$$

In conclusion, the results and methods presented in this thesis will be helpful tools in the future to experimentally realize these maximal intensity families of breathers as ways of compressing light pulses.

REFERENCES

[1] Y. V. Kartashov, B. A. Malomed, and L. Torner, Rev. Mod. Phys. **83**, 247 (2011).

[2] C. Kharif and E. Pelinovsky, Eur. J. Mech. -B/Fluids **22**, 603 (2003).

[3] P. a. E. M. P. Janssen, J. Phys. Oceanogr. **33**, 863 (2003).

[4] J. M. Dudley, F. Dias, M. Erkintalo, and G. Genty, Nat. Photonics **8**, 755 (2014).

[5] F. D. Zong, Y. S. Yan, and S. T. Shen, J. Phys. Soc. Japan **83**, 104002 (2014).

[6] N. N. Akhmediev and A. Ankiewicz, *Solitons Nonlinear Pulses and Beams* (Chapman & Hall, London, 1997).

[7] V. B. Matveev and M. A. Salle, *Darboux Transformations and Solitons* (Springer-Verlag, Heidelberg, 1991).

[8] C. Rogers and W. K. Schief, *Bäcklund and Darboux Transformations: Geometry and Modern Applications in Soliton Theory* (Cambridge University Press, 2002).

[9] S. A. Chin, O. A. Ashour, and M. R. Belic, Phys. Rev. E **92**, 063202 (2015).

[10] D. J. Kedziora, A. Ankiewicz, and N. Akhmediev, Phys. Rev. E **85**, 066601 (2012).

[11] N. N. Akhmediev and V. I. Korneev, Teor. i Mat. Fiz. **69**, 189 (1987).

[12] D. J. Kedziora, A. Ankiewicz, and N. Akhmediev, Eur. Phys. J. Spec. Top. **223**, 43 (2014).

[13] C. Mahnke and F. Mitschke, Phys. Rev. A **85**, 1 (2012).

[14] M. Erkintalo, K. Hammani, B. Kibler, C. Finot, N. Akhmediev, J. M. Dudley, and G. Genty, Phys. Rev. Lett. **107**, 253901 (2011).

[15] B. Frisquet, B. Kibler, and G. Millot, Phys. Rev. X **3**, 041032 (2013).

[16] A. Osborne, *Nonlinear ocean waves and the inverse scattering transform*, Vol. 97 (Academic Press, 2010).

[17] E. Pelinovsky and C. Kharif, *Extreme Ocean Waves*, Vol. 1 (Springer, 2015), p. 196.

[18] M. Onorato, S. Residori, U. Bortolozzo, A. Montina, and F. T. Arecchi, *Rogue waves and their generating mechanisms in different physical contexts*, 2013.

[19] C. Garrett and J. Gemmrich, Phys. Today **62**, 62 (2009).

[20] A. Chabchoub, N. Hoffmann, M. Onorato, and N. Akhmediev, Phys. Rev. X **2**, 011015 (2012).

[21] Y. V. Bludov, V. V. Konotop, and N. Akhmediev, Phys. Rev. A **80**, 033610 (2009).

[22] D. R. Solli, C. Ropers, P. Koonath, and B. Jalali, Nature **450**, 1054 (2007).

[23] A. Armaroli, C. Conti, and F. Biancalana, Optica **2**, 497 (2015).

[24] V. B. Efimov, A. N. Ganshin, G. V. Kolmakov, P. V. E. McClintock, and L. P. Mezhov-Deglin, Eur. Phys. J. Spec. Top. **185**, 181 (2010).

[25] N. Akhmediev, A. Ankiewicz, and J. M. Soto-Crespo, Phys. Rev. E **80**, 026601 (2009).

[26] K. B. Dysthe and K. Trulsen, Phys. Scr. **T82**, 48 (1999).

[27] N. Akhmediev, J. M. Soto-crespo, and A. Ankiewicz, Phys. Lett. A **373**, 2137 (2009).

[28] R. Hirota, J. Math. Phys. **14**, 805 (1973).

[29] Z. Yan, Chaos, Solitons & Fractals **16**, 759 (2003).

[30] R. Jackiw and S.-Y. Pi, Phys. Rev. Lett. **64**, 2969 (1990).

[31] K. Porsezian and V. C. Kuriakose, *Optical Solitons: Theoretical and Experimental Challenges* (Springer, 2008).

[32] A. Biswas and D. Milovic, Commun. Nonlinear Sci. Numer. Simul. **15**, 1473 (2010).

[33] D. J. Kedziora, A. Ankiewicz, and N. Akhmediev, Phys. Rev. E **84**, 056611 (2011).

[34] N. N. Akhmediev and N. V. Mitzkevich, IEEE J. Quantum Electron. **27**, 849 (1991).

[35] D. J. Kedziora, A. Ankiewicz, and N. Akhmediev, Phys. Rev. E **86**, 056602 (2012).

[36] V. S. Varadarajan, *Lie groups, Lie algebras, and their representations*, Vol. 102 (Springer-Verlag, 1984).

[37] H. Yoshida, Phys. Lett. A **150**, 262 (1990).

[38] E. Forest and R. D. Ruth, Phys. D **43**, 105 (1990).

[39] S. A. Chin, Celest. Mech. Dyn. Astron. **106**, 391 (2010).

[40] S. A. Chin, O. A. Ashour, S. N. Nikolic, and M. R. Belic, Phys. Rev. E **95**, 012211 (2016).

[41] S. A. Chin, O. A. Ashour, S. N. Nikolic, and M. R. Belic, Phys. Lett. A **380**, 3625 (2016).

[42] A. Chowdury, D. J. Kedziora, A. Ankiewicz, and N. Akhmediev, Phys. Rev. E **91**, 032928 (2015).

[43] D. J. Kedziora, A. Ankiewicz, and N. Akhmediev, Phys. Rev. E **84**, 056611 (2011).

[44] S. Wabnitz and B. Wetzel, Phys. Lett. A **378**, 2750 (2014).

[45] J. M. Dudley, G. Genty, F. Dias, B. Kibler, and N. Akhmediev, Opt. Express **17**, 21497 (2009).

[46] K. Hammani, B. Wetzel, B. Kibler, J. Fatome, C. Finot, G. Millot, N. Akhmediev, and J. M. Dudley, Opt. Lett. **36**, 2140 (2011).

[47] B. Frisquet, A. Chabchoub, J. Fatome, C. Finot, B. Kibler, and G. Millot, Phys. Rev. A **89**, 023821 (2014).

[48] N. N. Akhmediev, V. I. Korneev, and N. V. Mitskevich, Zh. Eksp. Teor. Fiz **8**, 159 (1987).

[49] T. B. Benjamin and J. E. Feir, J. Fluid Mech. **27**, 417 (1967).

APPENDIX A

MATLAB CODE FOR SOLVING THE NLSE

```
function [PSI, t, x, k] = solve(dx, Nt, Xmax, Lt, mult, psi_0)
   % INPUT:
   %       dx: evolution step
   %       Nt: Number of fourier modes/t-nodes
   %       Xmax: maximum simulation length
   %       Lt: Box size (usually periodic size for ABs).
   %       mult: Box size multiple
   %       psi_0: initial wave function
   % OUTPUT:
   %       PSI: spatiotemporal wavefunction matrix
   %       t: transverse variable
   %       x: evolution variable
   Nx = Xmax/dx;                              % Number of evolution nodes
   dt = Lt/Nt;                                % Tranverse step size
   t = (-Nt/2:1:Nt/2-1)'*dt;                  % Spatial grid points
   x = (0:dx:Xmax).';                         % Temporal grid points
   V = @(psi, t) (-1*abs(psi).^2);             % Define Potential
   psi = psi_0;                               % Find initial condition
   k = 2*(-Nt/2:1:Nt/2-1)'*pi/Lt;             % Wave number
   k2 = k.^2;                                 % Squares of wavenumbers
   PSI = zeros(length(x), length(t));         % Matrix to save evolution
   PSI(1, :) = psi;                           % Save first step

   for j = 1:Nx                              % Start time evolution
      PSI(j+1, :) = T2(PSI(j,:).', dx, k2, V, t, mult);  % Evolve 1 step
   end
```

Listing A.1: Main solver function

```
function [psi] = T2(psi, dx, k2, V, t, mult)
   pot = V(psi, t);                          % Calculate potential
   psi = exp(-1i * dx/2 * pot).*psi;         % Nonlinear calculation
   psi = fftshift(fft(psi));                 % FFT
   psi = exp(-1i * dx * k2/2).*psi;          % Linear calculation
   psi = ifft(fftshift(psi));                % Inverse FFT
   pot = V(psi, t);                          % Calculate potential
   psi = exp(-1i * dx/2 * pot).*psi;         % Nonlinear calculation

   % Kill off unwanted modes
   Nt = length(t);
   if mult > 1
      psi = fft(psi);
      for i = 2:Nt/2+1
         if(mod(i-1, mult) ~= 0)
            psi(i) = 0; psi(Nt - i  + 2) = 0;
         end
      end
      psi = ifft(psi);
   end
```

Listing A.2: Second order symplectic algorithm with mode-killing for generation of NL Talbot carpets

```
function psi = T4S(psi, dx, k2, V, t, mult)
   s = 2^(1/3);   os = 1/(2-s);
   ft = os; bt = -s*os; % Forward and backward factors

   psi = T2(psi, ft*dx, k2, V, t, mult);
   psi = T2(psi, bt*dx, k2, V, t, mult);
   psi = T2(psi, ft*dx, k2, V, t, mult);
```

Listing A.3: Fourth order symplectic algorithm